(UNCLASSIFIED TITLE)

PRELIMINARY AERODYNAMIC HEATING ANALYSIS
FOR THE APOLLO COMMAND MODULE

Prepared by

R. Gustafson
N. Thyson

RESEARCH AND ADVANCED DEVELOPMENT DIVISION
AVCO CORPORATION
Wilmington, Massachusetts

Technical Memorandum

RAD-TM-62-65

Letter Contract M2H43X-406012

Avco Report Series 802

THIS REPORT WAS PREPARED IN ACCORDANCE WITH NAA/S&ID
LETTER CONTRACT M2H43X-406012. IT IS SUBMITTED IN PARTIAL
FULFILLMENT OF THE CONTRACT AND IN ACCORDANCE WITH
NAA/S&ID PROCUREMENT SPECIFICATION MC304-0001 AND SID62-
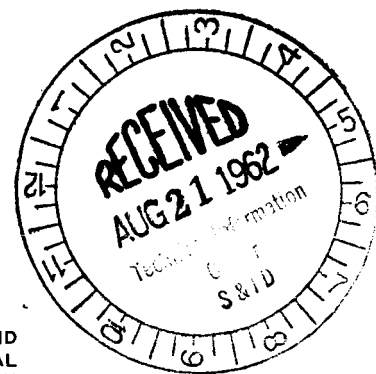420 (PARAGRAPH 4.0).

31 July 1962

CLASSIFICATION CHANGE

UNCLASSIFIED

To _____
By authority of _____ Date _____
Changed by _____
Classified Document Master Control Station, NASA
Scientific and Technical Information Facility

Prepared for

NORTH AMERICAN AVIATION, INC.
SPACE AND INFORMATION SYSTEMS DIVISION
Downey, California

(NASA-CR-127988) PRELIMINARY AERODYNAMIC
HEATING ANALYSIS FOR THE APOLLO COMMAND
MODULE (Avco Corp., Wilmington, Mass.) 63 p

N79-76124

Unclas
00/02 11697

~~CONFIDENTIAL~~

(UNCLASSIFIED TITLE)

PRELIMINARY AERODYNAMIC HEATING ANALYSIS
FOR THE APOLLO COMMAND MODULE
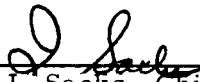
Prepared by

R. Gustafson
N. Thyson

RESEARCH AND ADVANCED DEVELOPMENT DIVISION
AVCO CORPORATION
Wilmington, Massachusetts

Technical Memorandum

RAD-TM-62-65

Letter Contract M2H43X-406012

Avco Report Series 802

31 July 1962

APPROVED

I. Sacks, Chief
Aerodynamics Section

J. E. Stevens, Manager
Engineering Analysis Department

E. Offenhartz
Project Manager
Apollo Research and Development

Prepared for

NORTH AMERICAN AVIATION, INC.
SPACE AND INFORMATION SYSTEMS DIVISION
Downey, California

~~CONFIDENTIAL~~

ABSTRACT

Aerodynamic heating is presented as preliminary design information for the Apollo command module heat shield.

Various theoretical approaches have been utilized to describe the heating distributions around the vehicle.

Experimental shock-tube test data are presented and comparisons are made with the theoretical predictions.

It is concluded that the various theories utilized present a valid approach for preliminary vehicle-design analysis.

CONTENTS

ILLUSTRATIONS

ILLUSTRATIONS (Cont'd)

ILLUSTRATIONS (Concl'd)

NOMENCLATURE

Symbols

C	transverse velocity gradient ratio, $\dfrac{dw_e/dz}{du_e/dx}$
H	enthalpy, $Btu\text{-}ft/sec^2\text{-}lb$
K	geometrical correction factor
M	Mach number
P	pressure, psf
$\dot{q}$	heating rate, $Btu/ft^2\text{-}sec$
r	recovery factor
s	surface distance, ft
R	radius, ft
R_e	Reynolds number
T	temperature, $^\circ R$
u	component of velocity in x direction
w	component of velocity in z direction
x, y, z	Cartesian coordinates
ϵ	emissivity
Δ	shock stand-off distance, ft
ρ	density, $slug/ft^3$
σ	Stefan-Boltzmann constant, 0.48×10^{-12} $Btu/ft^2\text{-}sec$ $^\circ R^4$
α	angle of attack, degrees

Subscripts

axisym   axisymmetric

nonaxisym   nonaxisymmetric

e   conditions at the edge of boundary layer or local conditions

o   standard atmospheric conditions

r   recovery conditions

s   stagnation conditions or stagnation point

cw   cold wall

hw   hot wall

∞ free-stream conditions

1   initial shock-tube conditions

t   isentropic total conditions

w   wall conditions

I. INTRODUCTION

The purpose of this report is to document the results of the aerodynamic heating studies for the North American Aviation, Inc., Phase I contract for the Apollo heat-shield design. The information presented herein describes some of the work performed to date, sets forth methods, and criteria for design, and indicates some problem areas which require special attention and additional study.

II. SUMMARY

The specified command module is a blunt-body configuration of the Mercury type with a major diameter of 154 inches. A sketch of the body is presented in figure 1 with dimensions and afterbody shape pertinent to the heating analysis. The body is trimmed to an angle of attack of 33° by an off-set center of gravity. To determine the effect of deviations from this attitude, an arbitrarily chosen angle of attack of 38° has been analyzed for the windward meridian.

The aerodynamic convective heating has been analyzed for the body points described in the NAA Procurement specification (reference 1) for the six specified re-entry trajectories. The trajectories specified to establish design criteria are determined by the bounds of the flight corridor defined by the deceleration limits of the crew, thermal and structural limits of the vehicle, and range requirements. The trajectory descriptions and heating comments, based on NAA data, are as follows:

1. Trajectory 1 is a typical lunar overshoot re-entry and results in the highest integrated heat load to the vehicle.

2. Trajectory 2 is a maximum-range lunar undershoot re-entry which results in a high heat flux and heat load.

3. Trajectory 3 is a minimum-range lunar undershoot re-entry which results in a high heat flux and heat load.

4. Trajectory 4 is a minimum-range, 20-g, special lunar re-entry trajectory which results in the highest heat flux.

5. Trajectory 5 is a 20-g maximum-range orbital re-entry trajectory which results in the highest orbital heat flux.

6. Trajectory 6 is a long-range oscillatory orbital re-entry trajectory which results in the highest integrated orbital heat load.

Experimental heating distributions over the body were obtained in the Avco shock tube. Comparisons between the experimental and theoretical heating distributions are in good agreement.

The second primary source of heat transfer to the command module is radiative heating from the flow field. Radiative heat fluxes were predicted on the basis of radiation from a semi-infinite slab of hot air having a thickness equal to the shock stand-off distance. The emissivity of the air was obtained from the works of Kivel and Bailey (reference 2). Shock detachment distances were obtained by

AVCO
Research & Advanced Development

POINT	X	Z
1	14.6	71.6
2	3.3	37.4
3	0.0	0.0
4	5.9	44.0
5	15.8	72.4
6	25.7	76.6
7	31.1	73.0
8	49.3	61.0
9	67.8	48.6
10	89.3	34.5
11	108.8	22.0
12	25.7	0.0
13	49.3	0.0
14	67.8	0.0
15	89.3	0.0
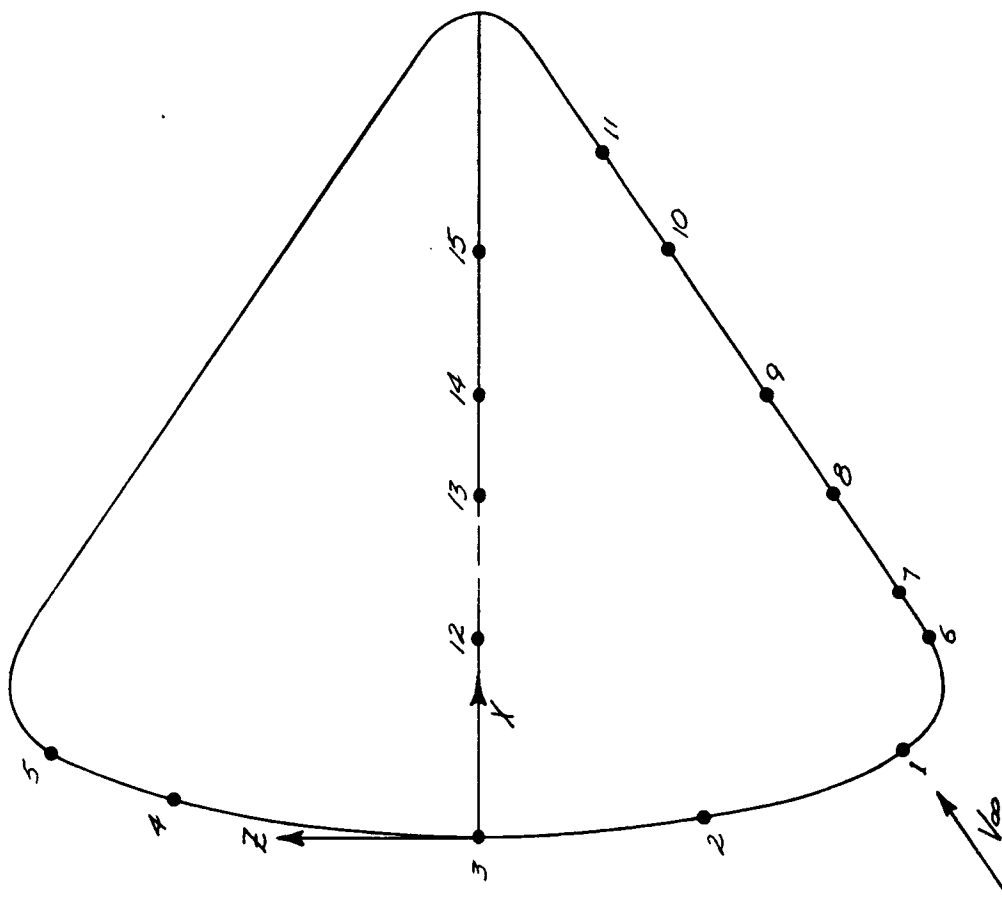
Figure 1 LOCAL BODY POINTS FOR APOLLO SHAPE

-3-

correlating JPL Schlieren test data with Kaattari's (reference 3) theoretical predictions. The radiative-heating estimates are a conservative evaluation of the actual radiation heat flux caused by 1) the semi-infinite slab assumption which overestimates the volume and temperature level of radiant gases, and 2) neglecting of self-absorption of the radiant energy by the gas.

III. CONVECTIVE HEATING

The convective heating presented in this report is cold-wall convective heating for a wall temperature of 5000°R. The cold-wall convective heat transfer rate by definition is

$$\dot{q}_{cw} = \frac{\dot{q}_{hw}}{\dfrac{Hr}{Hs} - \dfrac{Hw}{H_s}}$$

Because of the nature of the theories used in the analysis, the wall temperature must be specified, since the boundary conditions are evaluated at the wall as well as at the edge of the boundary layer.

The stagnation-point heating was calculated for all six re-entry trajectories (figures 2 and 3). For design information, the heating distributions around the vehicle have been determined for trajectory 1 which results in the highest integrated heat load to the vehicle and trajectory 4 which results in the highest heat flux.

The aerodynamic heating analysis has been restricted to real gases in equilibrium. The flow over the body has been taken as basically laminar for all body points, except trajectory 4 where the flow becomes turbulent on the spherical face at approximately the time of maximum heat flux. For all other points the largest integrated heat load occurs in laminar flow; transition occurs late in the trajectories when heating rates are too low to be of importance.

The surface-pressure distributions used in the heating analysis have been obtained from JPL and Langley wind tunnel test data (figures 4 and 5). The averaged surface-pressure distributions from the test data are presented in nondimensional form. The local surface-pressure ratioed to the stagnation pressure is essentially independent of Mach number and gas composition. This is confirmed by pressure data for a similar body tested at JPL ($M = 9.5$) and in the Cornell shock tunnel ($M = 18.70$) (figure 6).

The cold-wall equilibrium convective heating was calculated for the following re-entry trajectories at the body points indicated:

NAA Body Points	NAA Trajectories
1 (Stagnation Point)	1, 2, 3, 4, 5 and 6
2 through 15	1 and 4
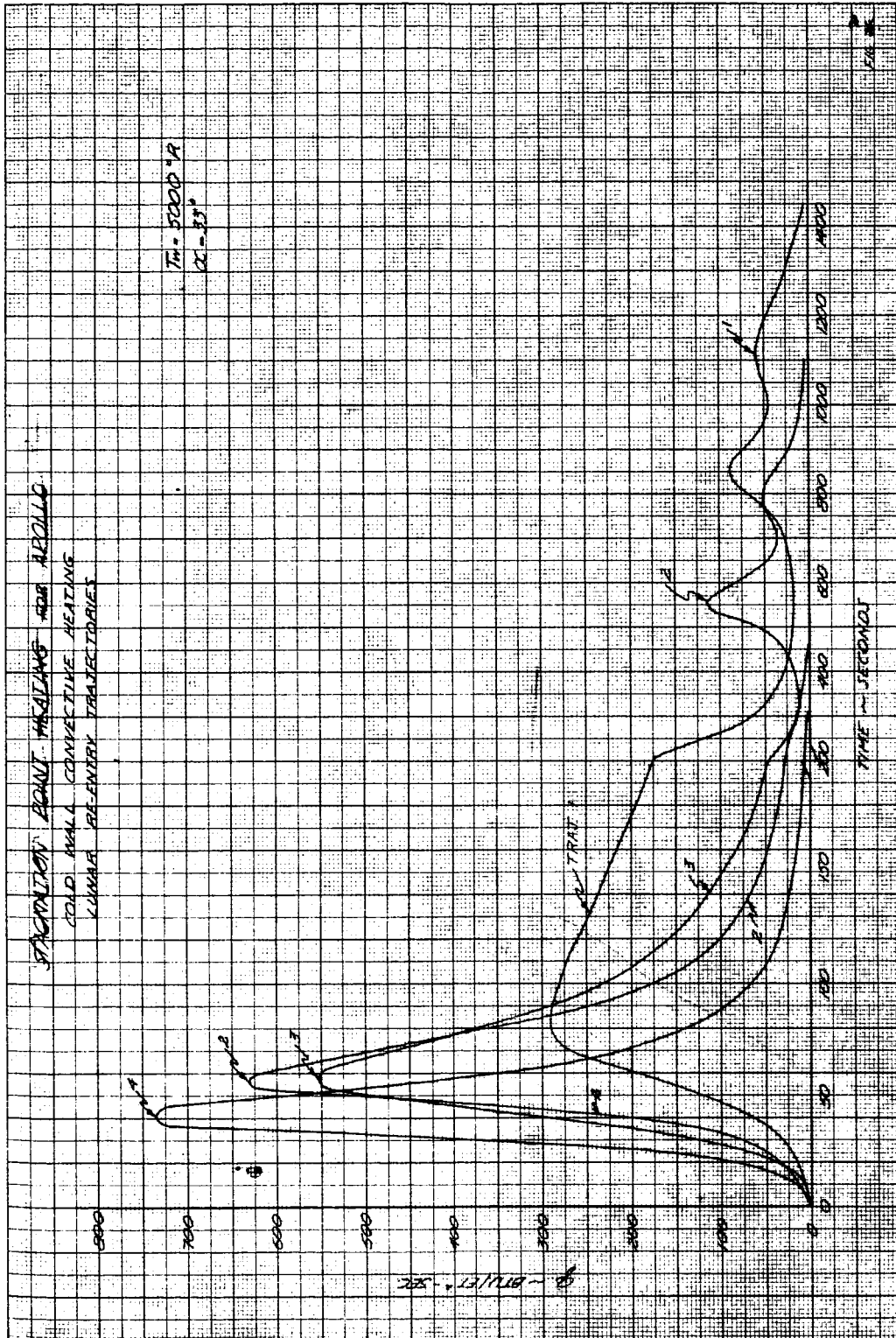
Figure 2 STAGNATION-POINT HEATING FOR APOLLO (LUNAR
RE-ENTRY TRAJECTORIES)

-6-
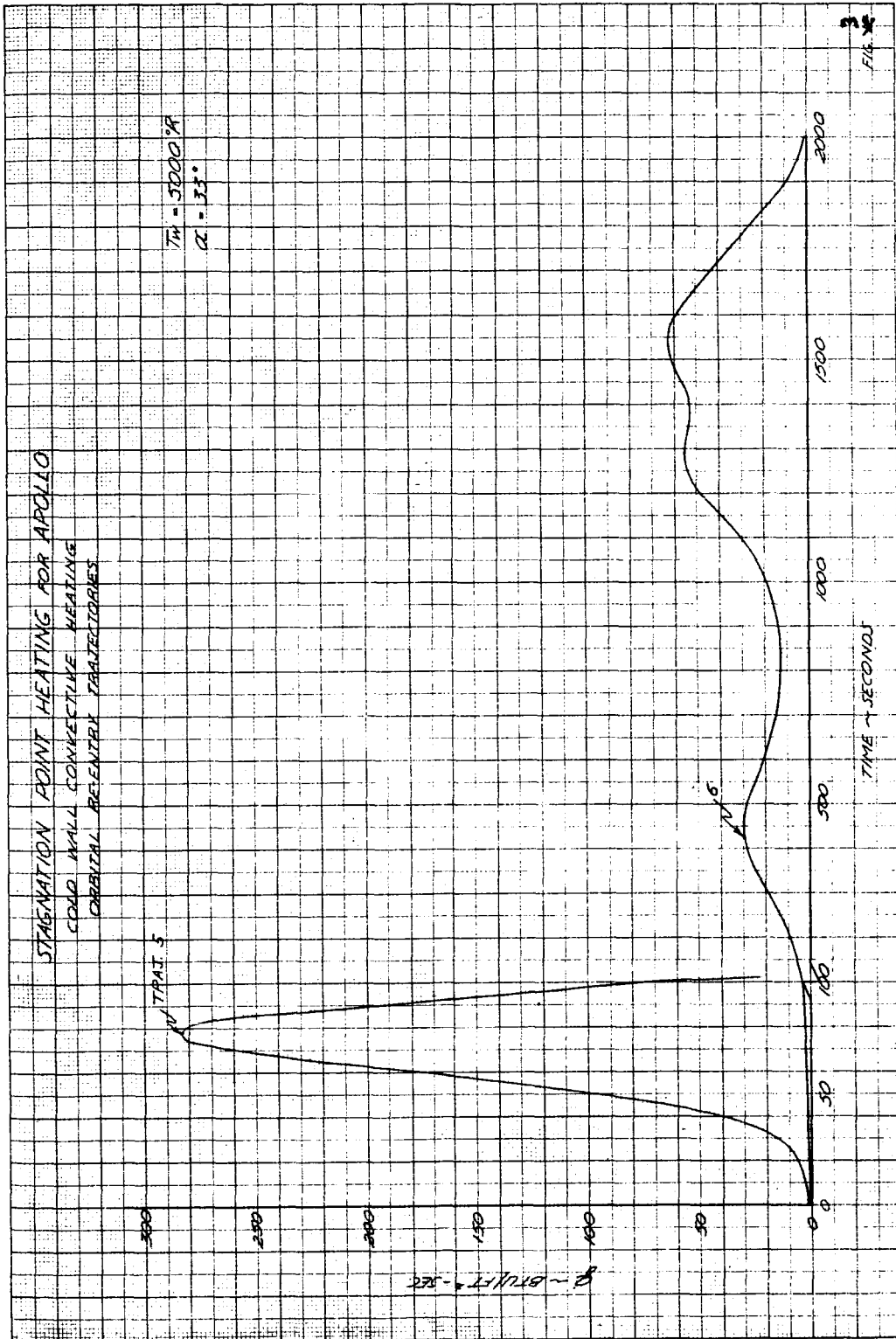
Figure 3 STAGNATION-POINT HEATING FOR APOLLO (ORBITAL RE-ENTRY TRAJECTORIES)

-7-

APOLLO STATIC PRESSURE DISTRIBUTION

$\alpha = 33°$

$\lambda = 0°$

(TEST DATA AVERAGE $M = 6.42, 7.37, 9.03$)

-3.79
+1.91

$S = 0$ AT STAG PT

LEEWARD   WINDWARD

1.0

.8

.6

$\frac{P}{P_{STAG}}$

.4

.2

LANGLEY TEST DATA
$M_\infty = 8, \alpha = 38°$

0

-4   -3   -2   -1   0   +1   +2

$\frac{S}{R}$

FIG 4
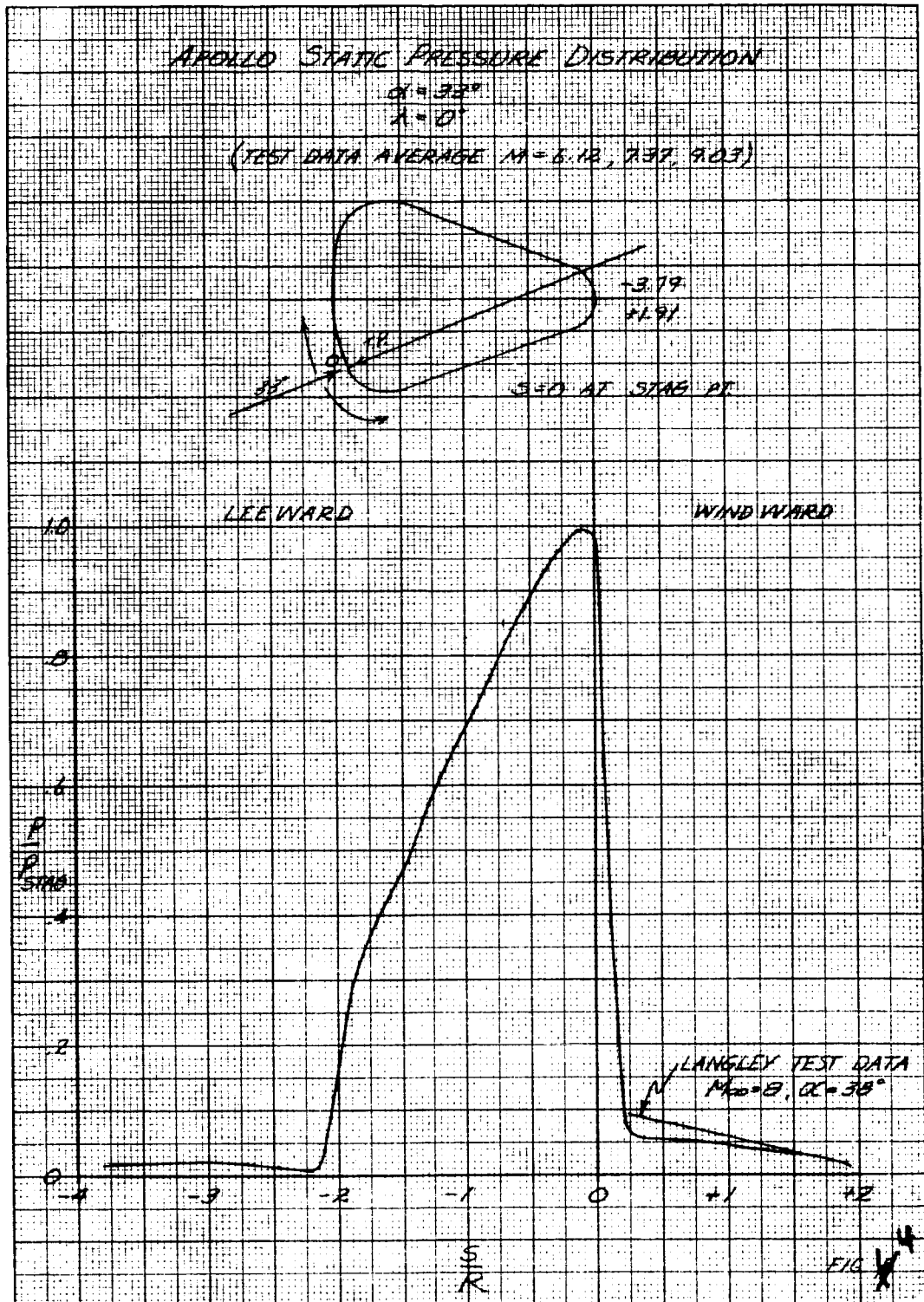
Figure 4   APOLLO STATIC-PRESSURE DISTRIBUTION $\phi = 0°$

AVCO
Research & Advanced Development
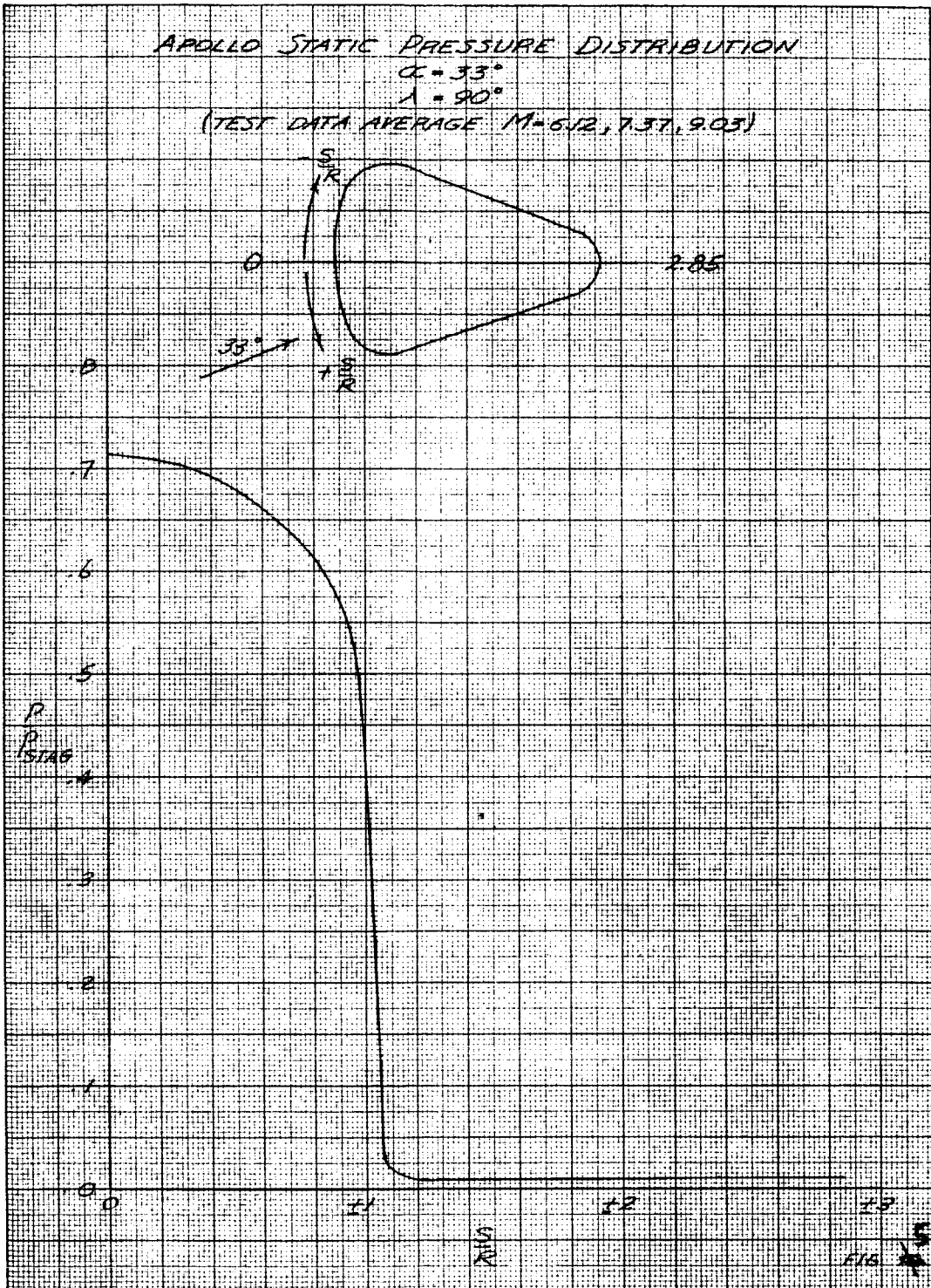
Figure 5 APOLLO STATIC-PRESSURE DISTRIBUTION $\phi = 90°$

-9-

AVCO
Research & Advanced Development

Figure 6 SURFACE-PRESSURE DISTRIBUTION

-10-

Figure 1 illustrates the location of the body points and figures 7 through 12 show the re-entry trajectories.

METHOD OF HEATING ANALYSIS
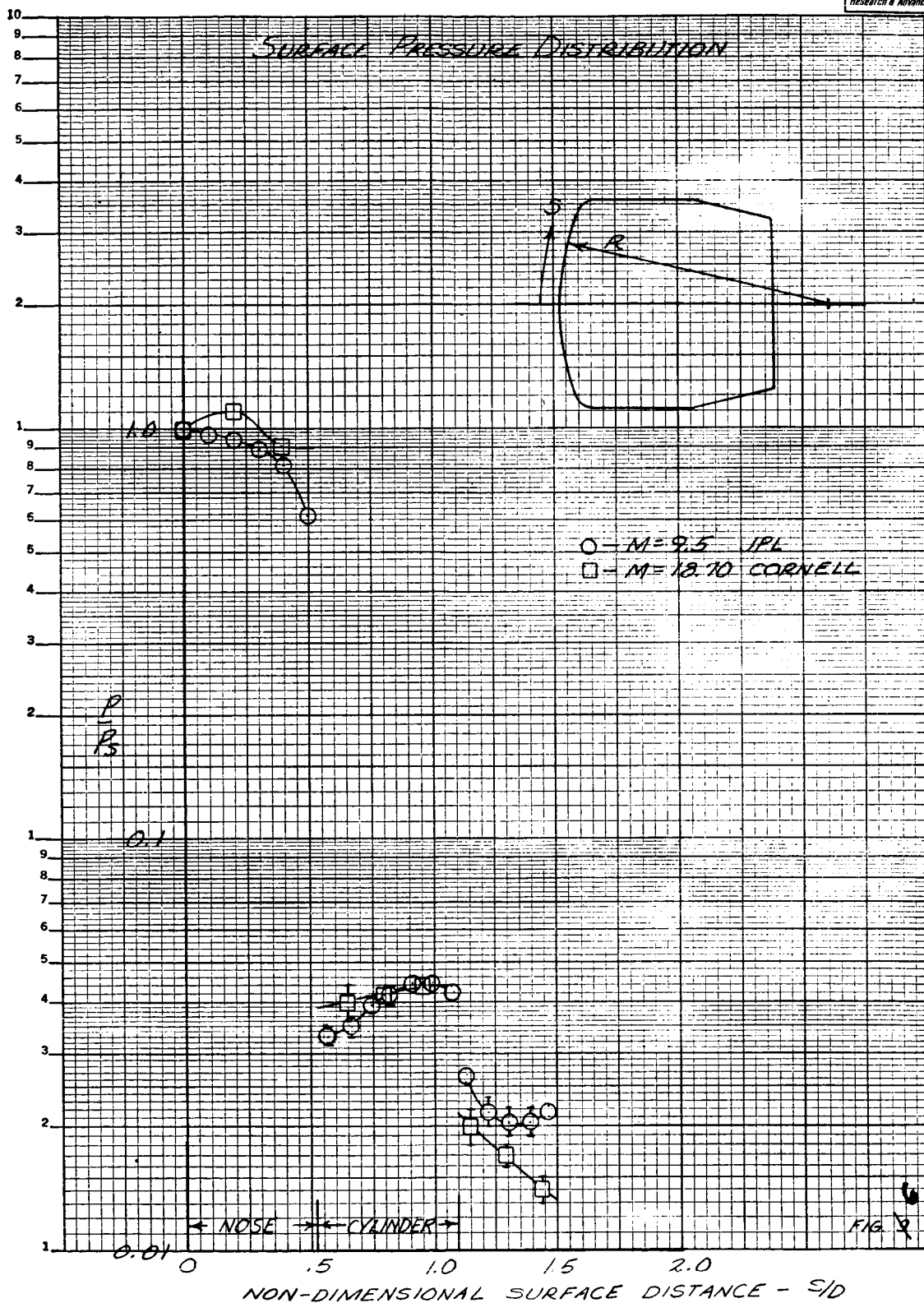
1.   <u>Point 1 (Stagnation Point)</u>

The stagnation-point heating was calculated for a three-dimensional non-axisymmetric stagnation point. This nonaxisymmetric heating was computed by appropriately modifying the axisymmetric heating of Fay and Riddell (reference 4) through the following relation of Reshotko (reference 5)

$$\dot{q}_{s_{nonaxisym}} = \dot{q}_{s_{axisym}} \left(\frac{1 + C}{2} \right)^{1/2}$$

where

$$C = \frac{dw_e/dz}{du_e/dx} = \frac{R_x}{R_z} \qquad 0 \leq C \leq 1 \quad .$$

It should be noted that Reshotko's result is believed to be in error; that is, the radius ratio exponent should be "1" and not "1/2." The axisymmetric heating is

$$\dot{q}_{s_{axisym}} \quad \alpha \left(\frac{1}{R_x} \right)^{1/2} \quad .$$

For this analysis, the following values of R_x and R_z were used:

R_x = 7. 7 inches

R_z = 77 inches

2.   <u>Spherical Face, Zero Meridian (Points 2, 3, 4 and 5)</u>

Heating along the zero meridian of the spherical face, was analyzed in accordance with the following theories:

a.   Laminar Flow - Similarity Theory (Reference 6)

The flow along this line should nearly be axisymmetric. Hence, the geometric factor, K, used in the laminar similarity theory, was taken equal to one.

-11-

AVCO
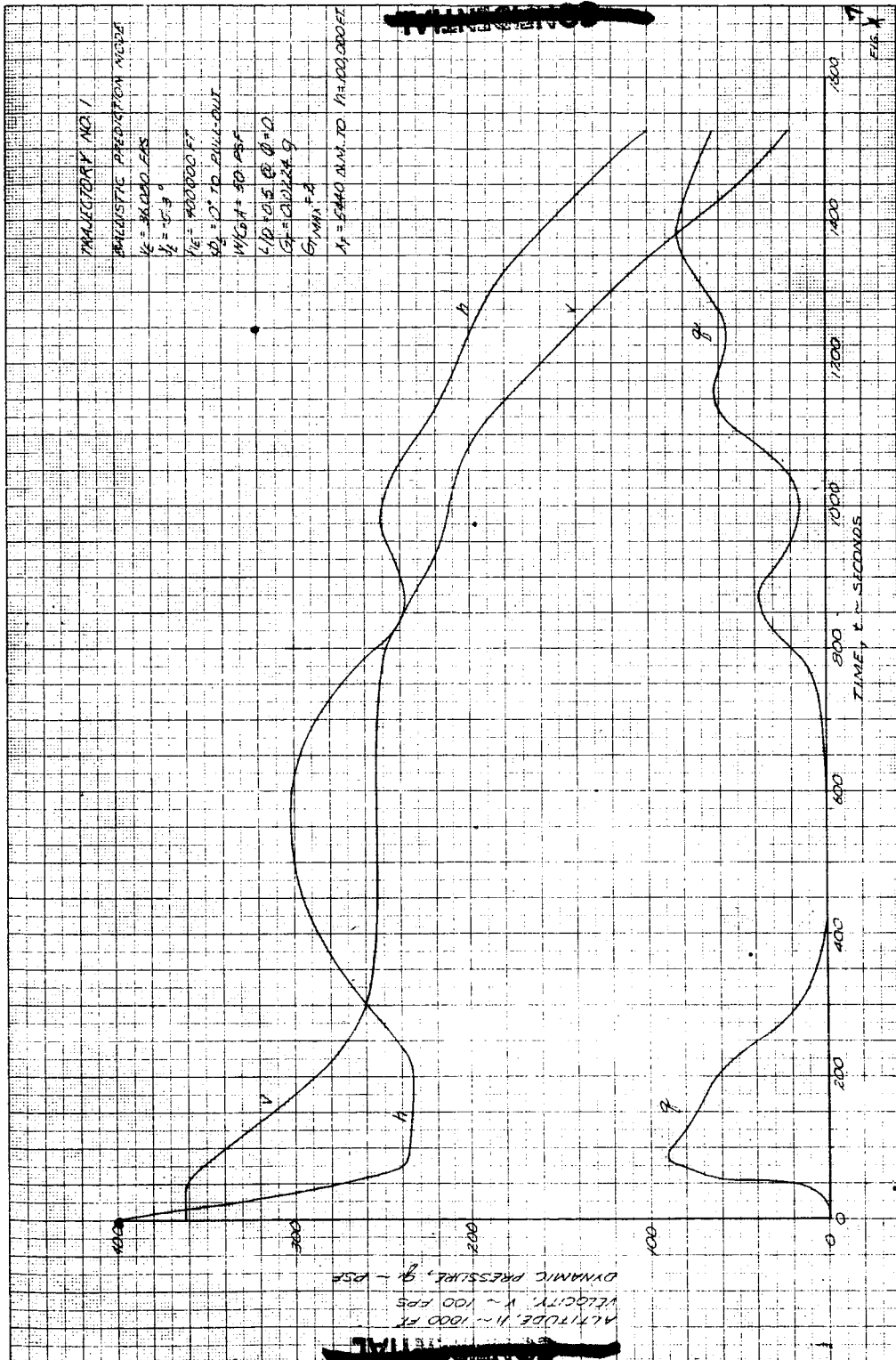Research & Advanced Development

Figure 7 TRAJECTORY NO. 1
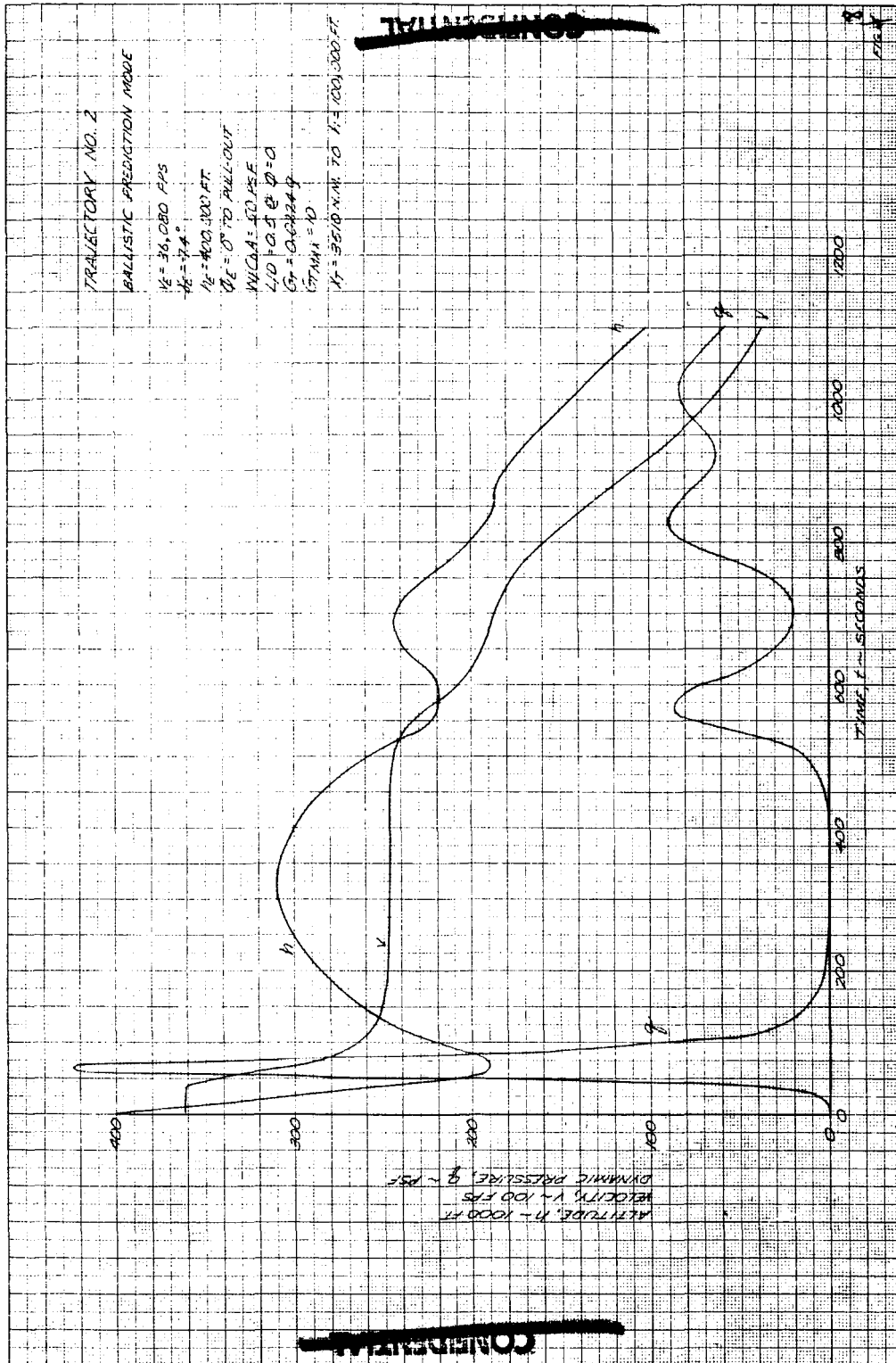
Figure 8 TRAJECTORY NO. 2
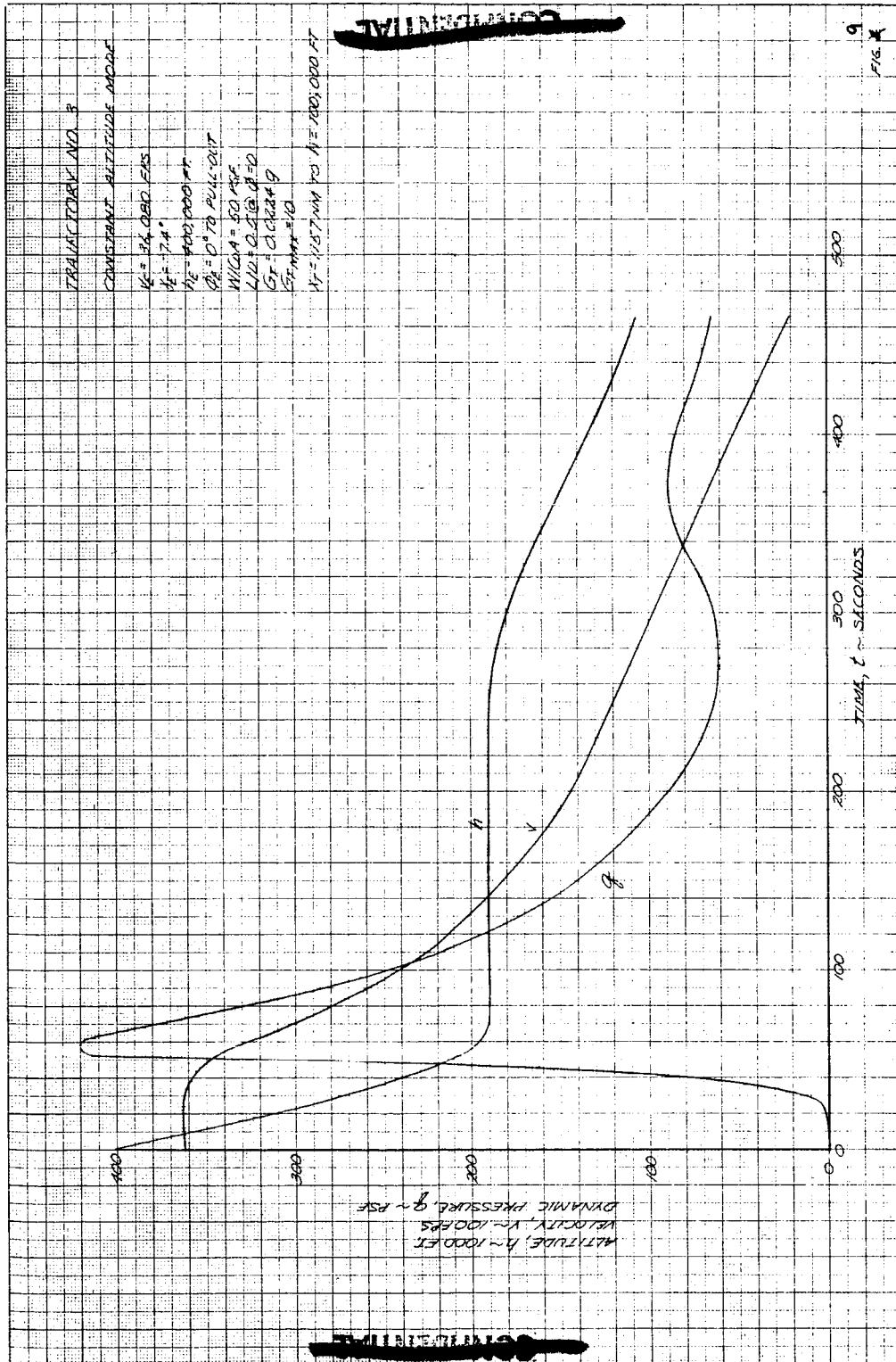
Figure 9   TRAJECTORY NO. 3

-14-
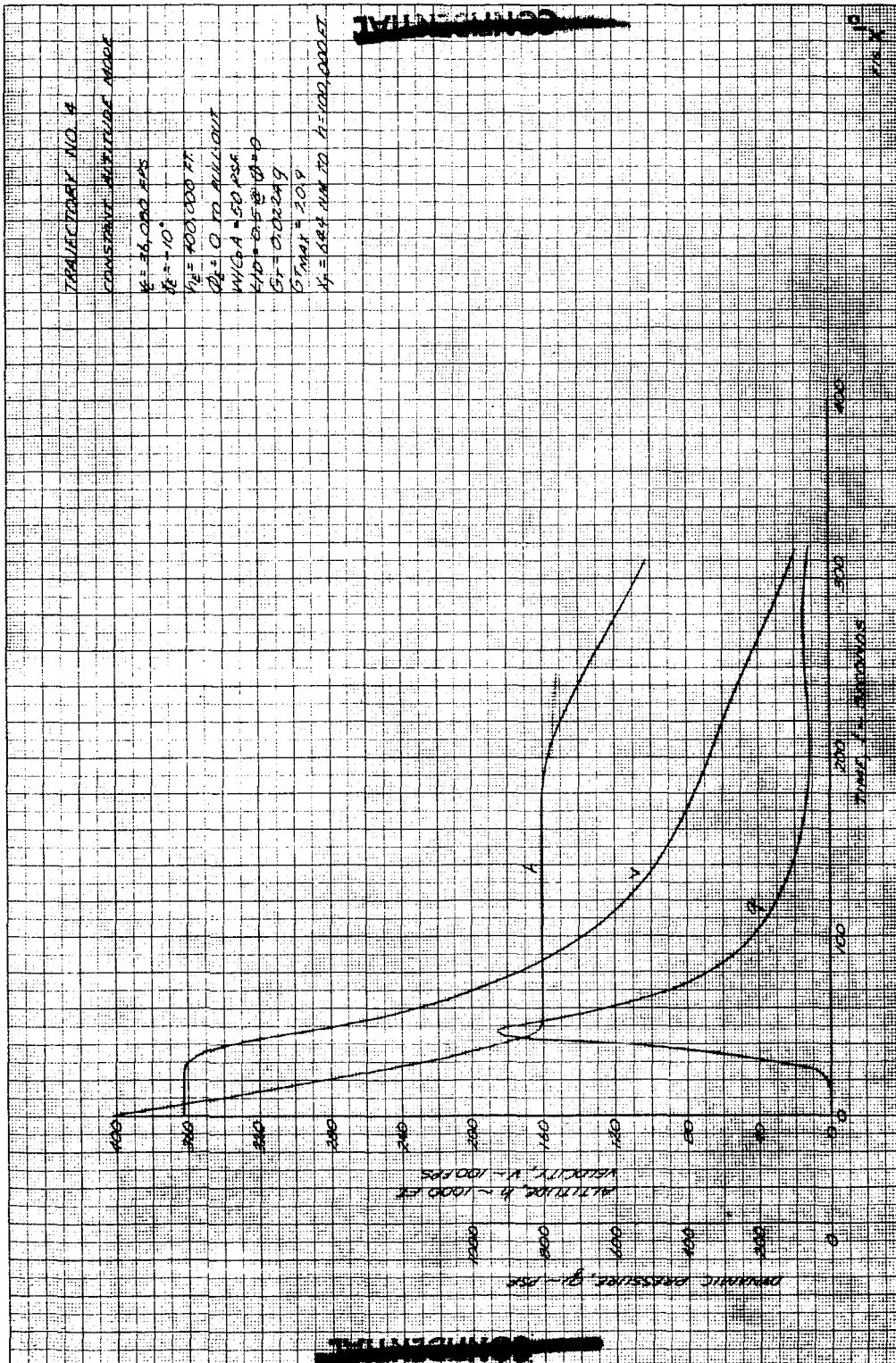
Figure 10 TRAJECTORY NO. 4

Figure 11 TRAJECTORY NO. 5

-16-

AVCO
Research & Advanced Development
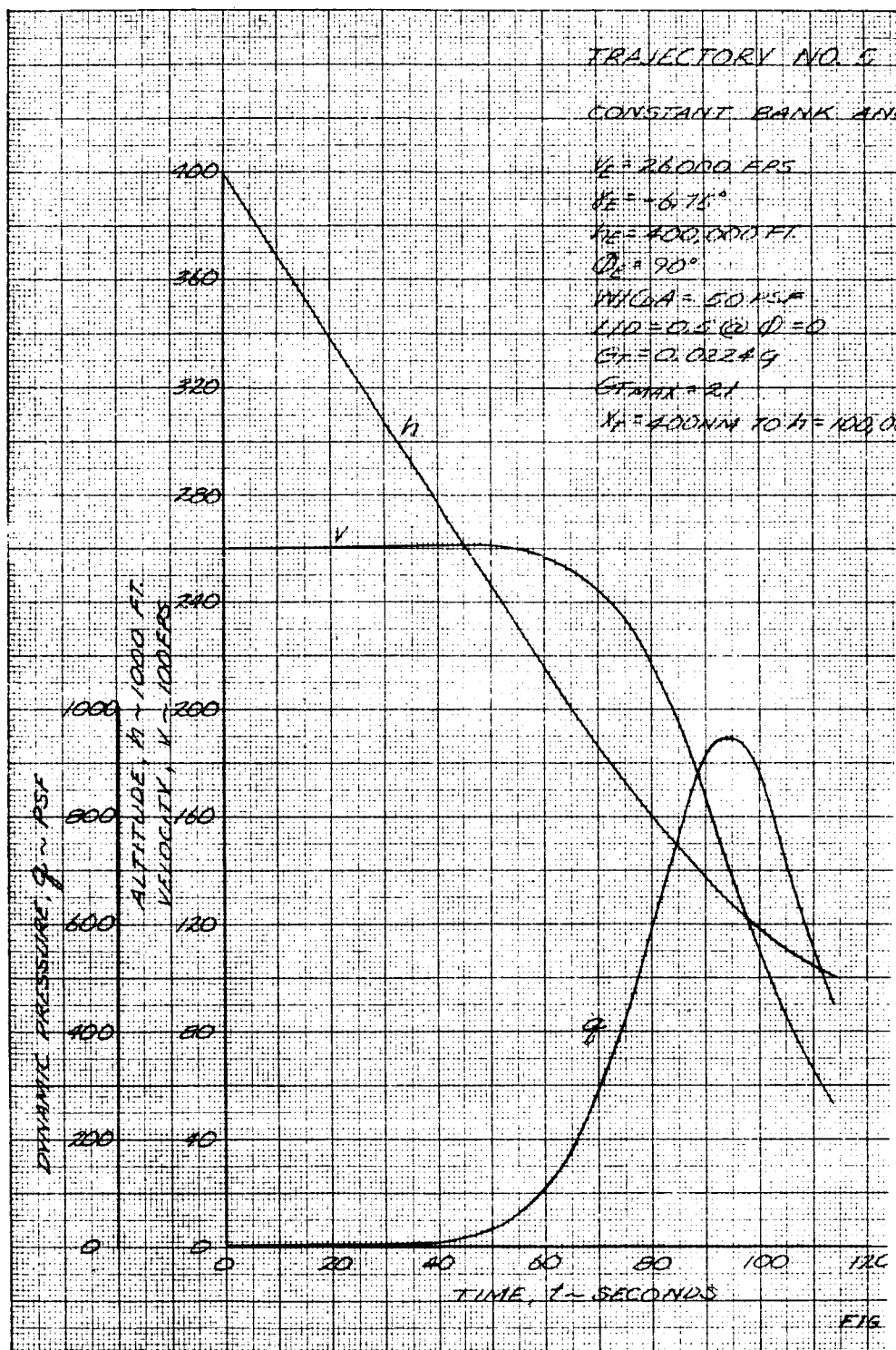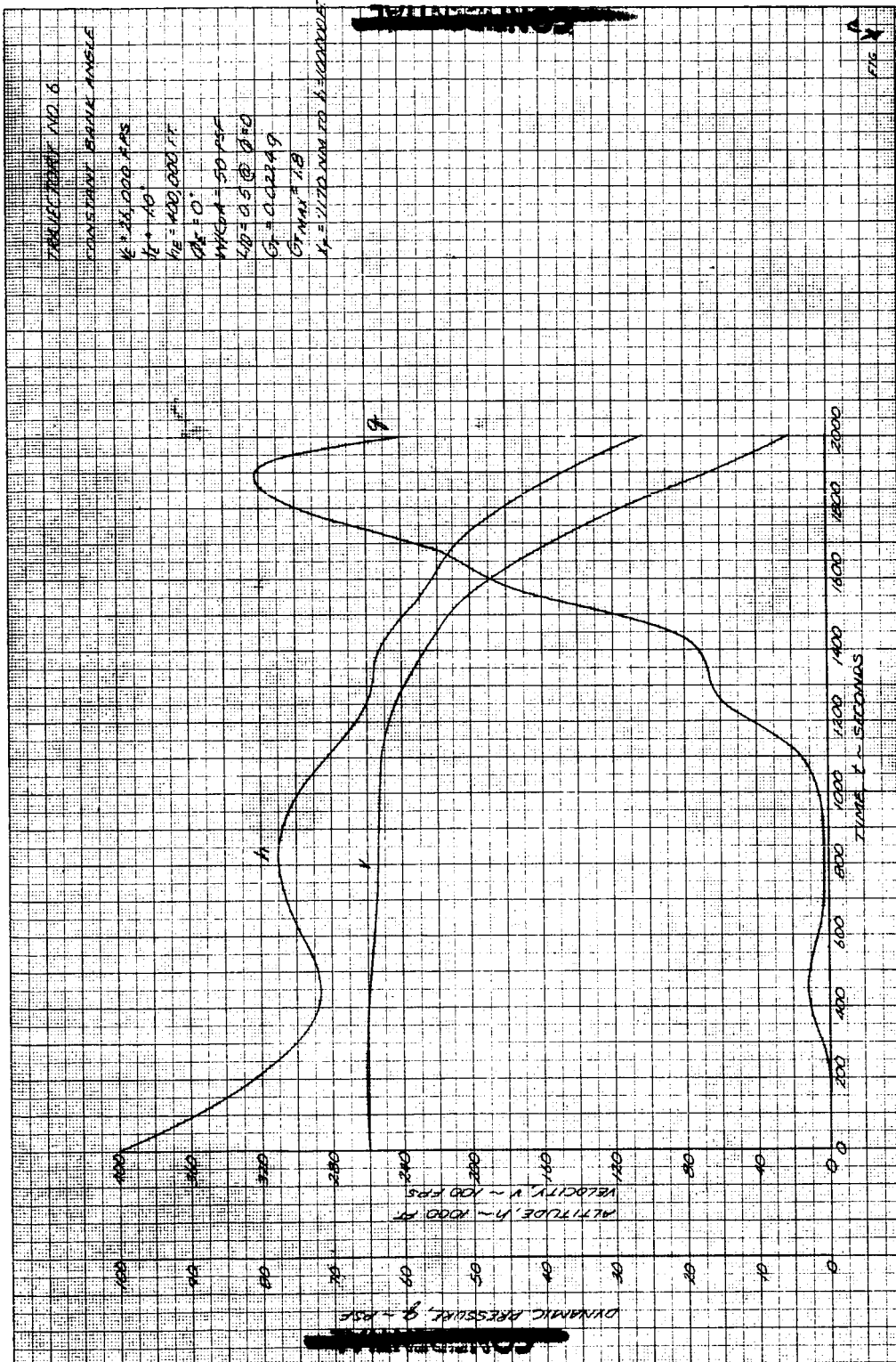
Figure 12 TRAJECTORY NO. 6

b. Turbulent Flow - Turbulent Flat Plate Reference Enthalpy (Reference 7)

An average pressure distribution (figure 4), based on the JPL and Langley wind tunnel tests, was used in connection with the normal shock entropy to obtain the external flow at these points. The nondimensional pressure distribution (P/P_s) was taken to be constant throughout the trajectories. The local Reynolds number value, $R_{ex} = 3 \times 10^5$ was used as the criterion for turbulent flow. This method of obtaining the external flow and the Reynolds number criterion for turbulent flow was used throughout all heating analysis.

3. <u>Windward Shoulder, Zero Meridian</u>

The flow along the zero meridian of the windward shoulder approaches the two-dimensional flow of a cylinder. Hence, the geometric factor, K, used in the laminar similarity theory, approaches zero. The value used for the K in this analysis was obtained as follows:

$$\dot{q}_{s_{nonaxisym}} = \dot{q}_{s_{axisym} \atop K=1} \left(\frac{1+C}{2}\right)^{1/2}$$

where

$$\dot{q}_{axisym \atop K=1} \ a \ (2)^{\frac{K=1}{2}} \left(\frac{1}{R_x}\right)^{1/2}$$

Postulate a

$$\dot{q}_{s \atop K} \ a \ (2^{K/2}) \left(\frac{1}{R_x}\right)^{1/2}$$

Then

$$\frac{\dot{q}_{s \atop K}}{\dot{q}_{s_{axisym} \atop K=1}} = \frac{2^{K/2}}{2^{1/2}} = 2^{\frac{K-1}{2}}$$

-18-

Set

$$\dot{q}_s \atop K = \dot{q}_{s_{nonaxisym}}$$

$$\left[\dot{q}_{s_{axisym} \atop K=1} \right] 2^{\frac{K-1}{2}} = \left[\dot{q}_{s_{axisym} \atop K=1} \right] \left[\frac{1+C}{2} \right]^{1/2}$$

$$2^{\frac{K-1}{2}} = \left[\frac{1+C}{2} \right]^{1/2}$$

$$K = 0.134$$

Since the flow around the shoulder is close to the stagnation point, turbulent flow does not occur. Hence, only a laminar heating analysis is required.

4. Windward Conical Afterbody, Zero Meridian (Points 6, 7, 8, 9, 10 and 11)

The following theories were used to analyze the heating along the zero-meridian of the windward conical afterbody:

a. Laminar Flow - Laminar Flat Plate Reference Enthalpy (Reference 7)

b. Turbulent Flow - Turbulent Flat Plat Reference Enthalpy (Referency 7)

The external flow was obtained from the nondimensional pressure distribution and the Reynolds number criterion for turbulent flow was $R_{ex} = 3 \times 10^5$.

5. Conical Afterbody, 90-Degree Meridian (Points 12, 13, 14 and 15)

Heating along the 90-degree meridian of the conical afterbody was calculated by the following theories:

a. Laminar Flow - Laminar Flat Plate Reference Enthalpy (Reference 7)

b. Turbulent Flow - Turbulent Flat Plate Reference Enthalpy (Reference 7)

The reference enthalpy method was employed for the Apollo shape at 0-degree angle of attack. The average pressure distribution at 33 degrees was determined from JPL-averaged test data (figure 5). This approach gives the correct external flow at these points. Only the surface distance from the stagnation point to the points along the 90-degree meridian would be in error. However, there should be little difference between the surface distance from the stagnation point to points along the 90-degree meridian at a 0-degree angle of attack and at a 33-degree angle of attack.

The cold-wall equilibrium convective heating is presented in the figures as listed in Table I:

<u>TABLE I</u>

LIST OF CONVECTIVE HEATING FIGURES

Figure	α	Body Points	Trajectories
2	33	1 (Stag Pt)	1, 2, 3, and 4
3	33	1 (Stag Pt)	5 and 6
13	33	2, 3, 4 and 5	1
14	33	2, 3, 4 and 5	4
15	33	6, 7, 8, 9, 10 and 11	1
16	38	6, 7, 8, 9, 10 and 11	1
17	33	6, 7, 8, 9, 10 and 11	4
18	38	6, 7, 8, 9, 10 and 11	4
19	33	12, 13, 14 and 15	1
20	33	12, 13, 14 and 15	4

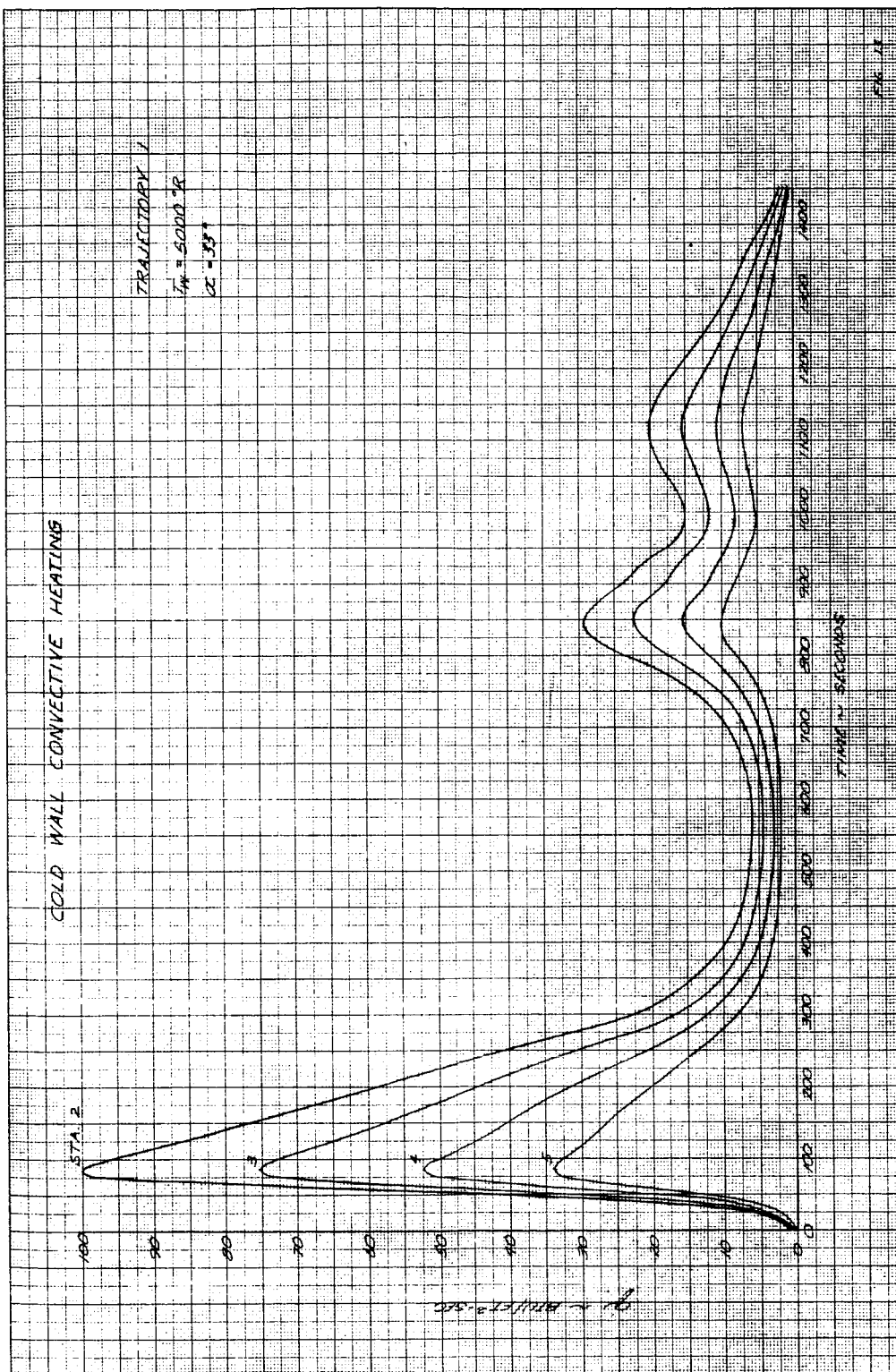Figures 21 through 26 show typical local Reynolds number variations for various trajectories.

Figure 13 COLD-WALL CONVECTIVE HEATING (PTS. 2-5, α = 33°, TRAJ. 1)

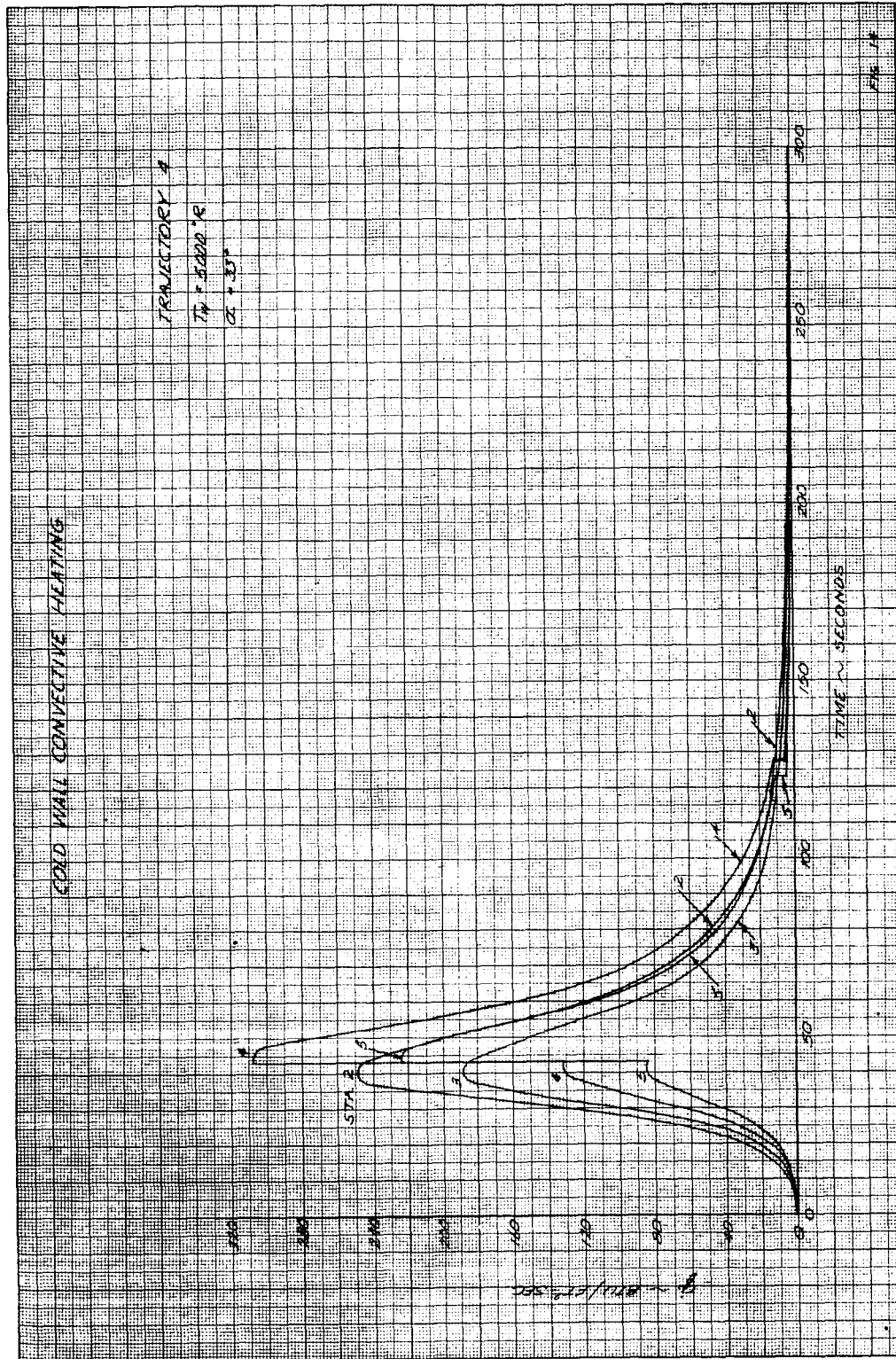Figure 14 COLD-WALL CONVECTIVE HEATING (PTS. 2-5, $\alpha = 33^\circ$, TRAJ. 4)

Figure 15 COLD-WALL CONVECTIVE HEATING (PTS. 6-11, $a = 33^\circ$, TRAJ. 1)

Figure 16 COLD-WALL CONVECTIVE HEATING (PTS. 6-11, $\alpha = 38°$, TRAJ. 1)

-24-
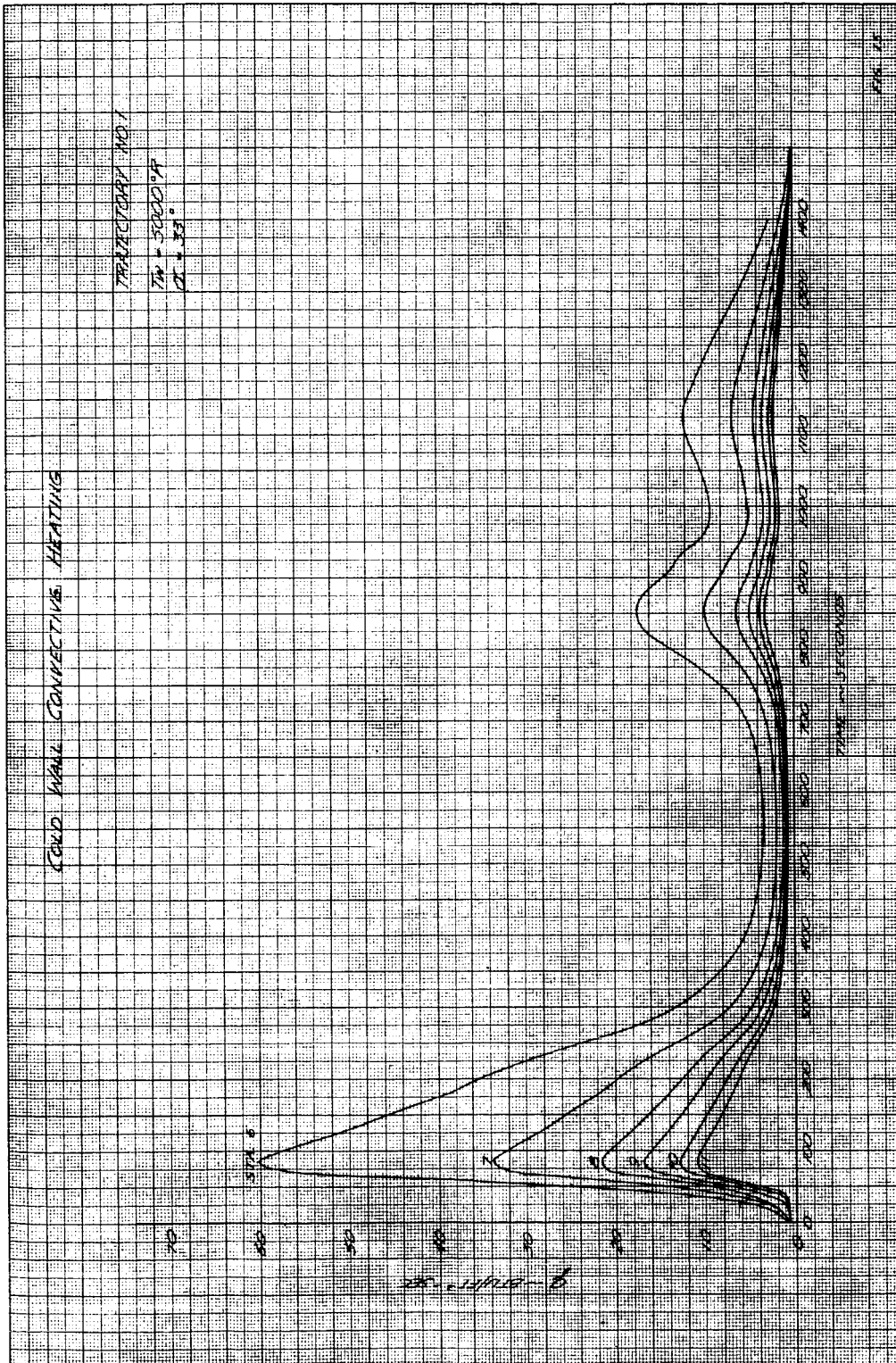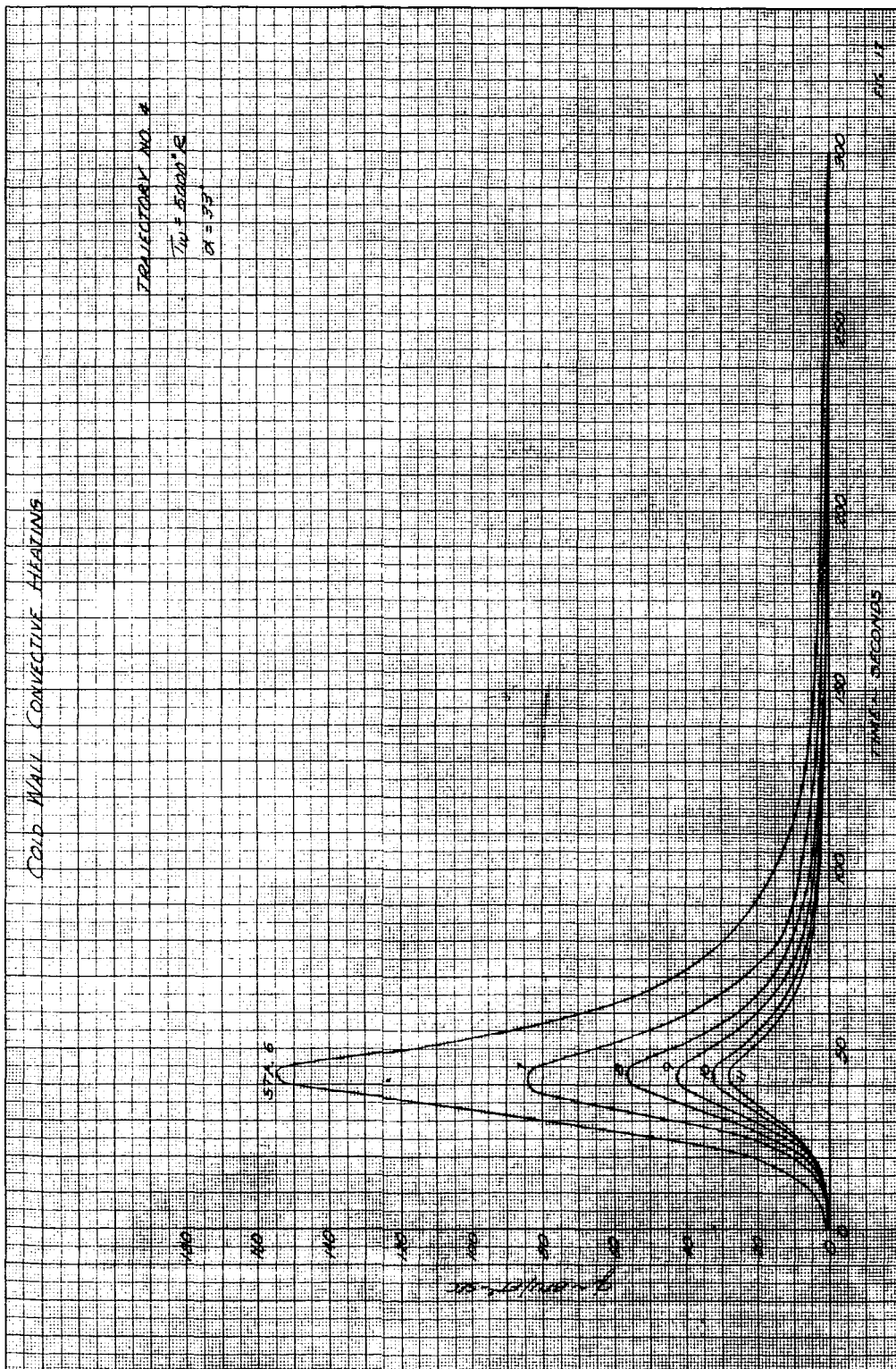
Figure 17 COLD-WALL CONVECTIVE HEATING (PTS. 6-11, $\alpha = 33°$, TRAJ. 4)
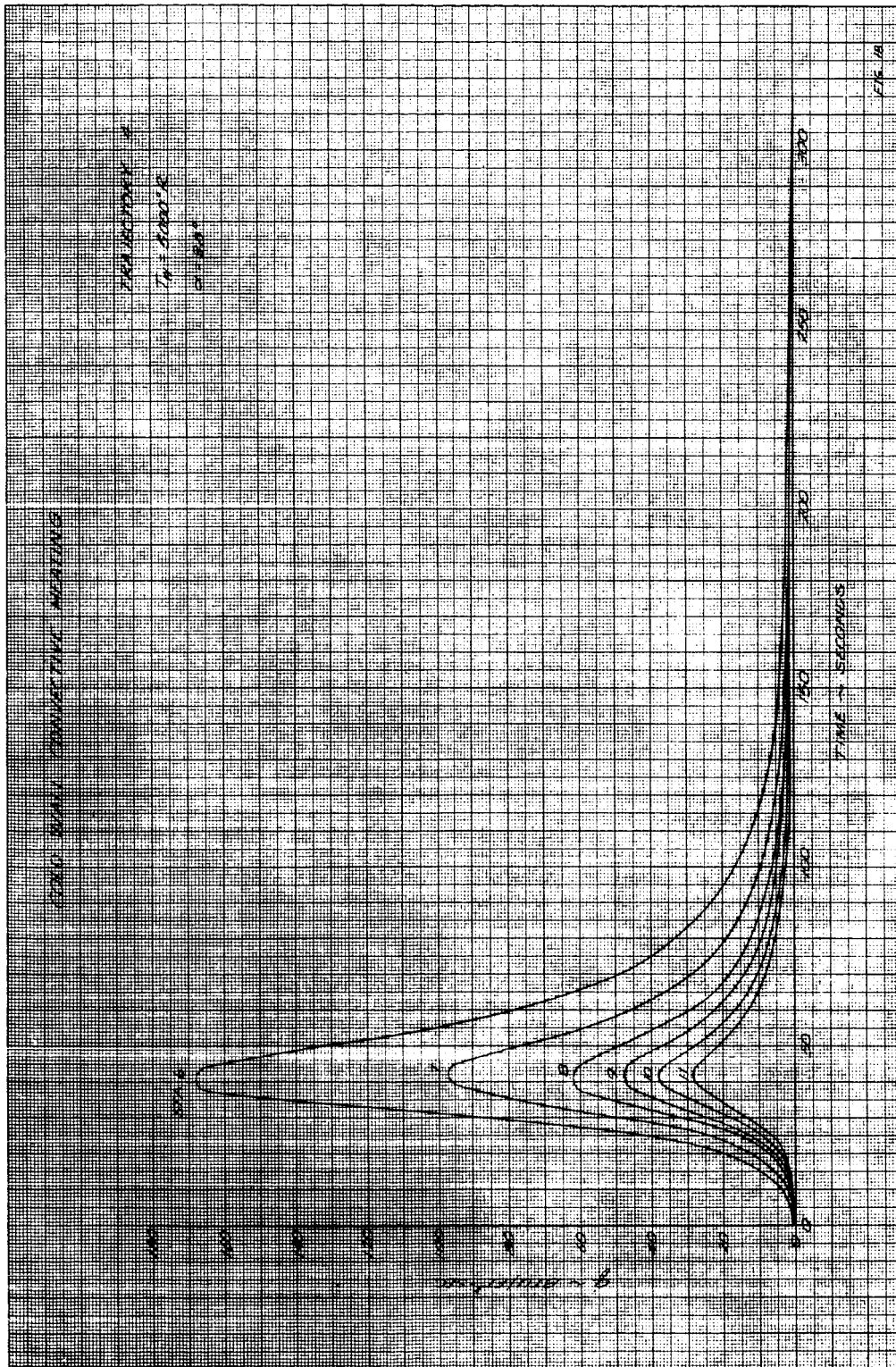
Figure 18 COLD-WALL CONVECTIVE HEATING (PTS. 6-11, $\alpha = 38°$, TRAJ. 4)

-26-
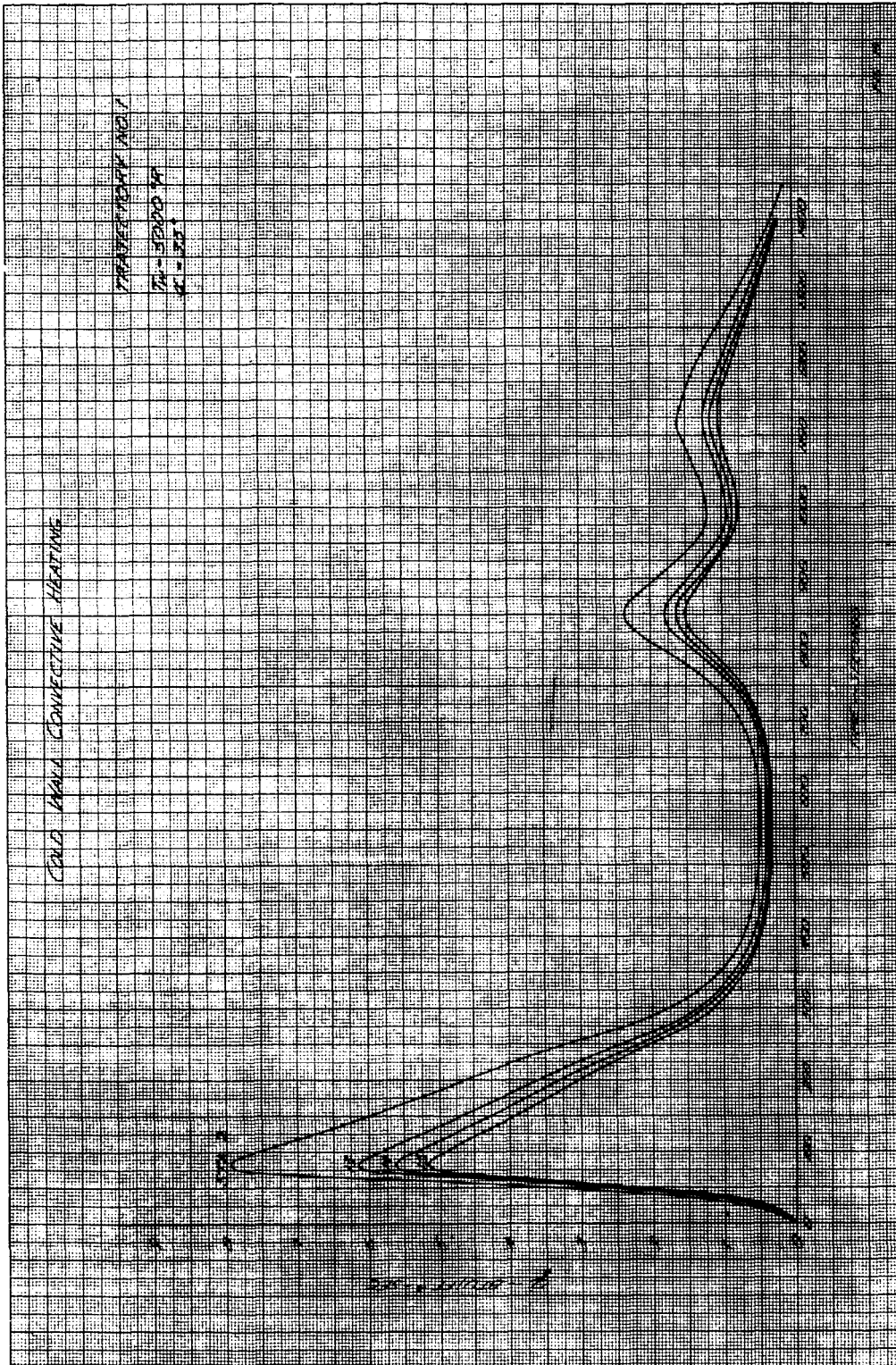
Figure 19 COLD-WALL CONVECTIVE HEATING (PTS. 12-15, $\alpha = 33^\circ$, TRAJ. 1)

-27-

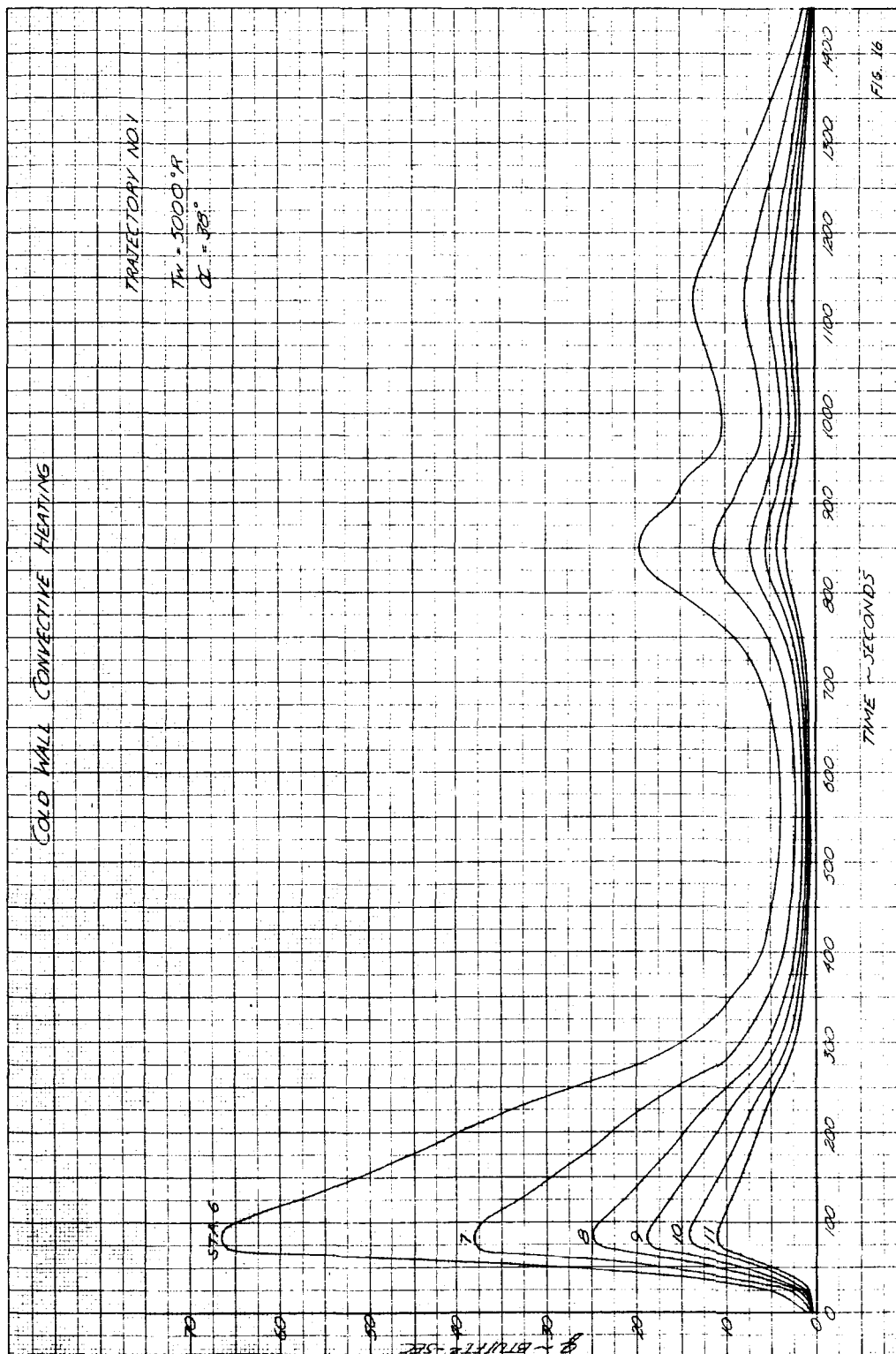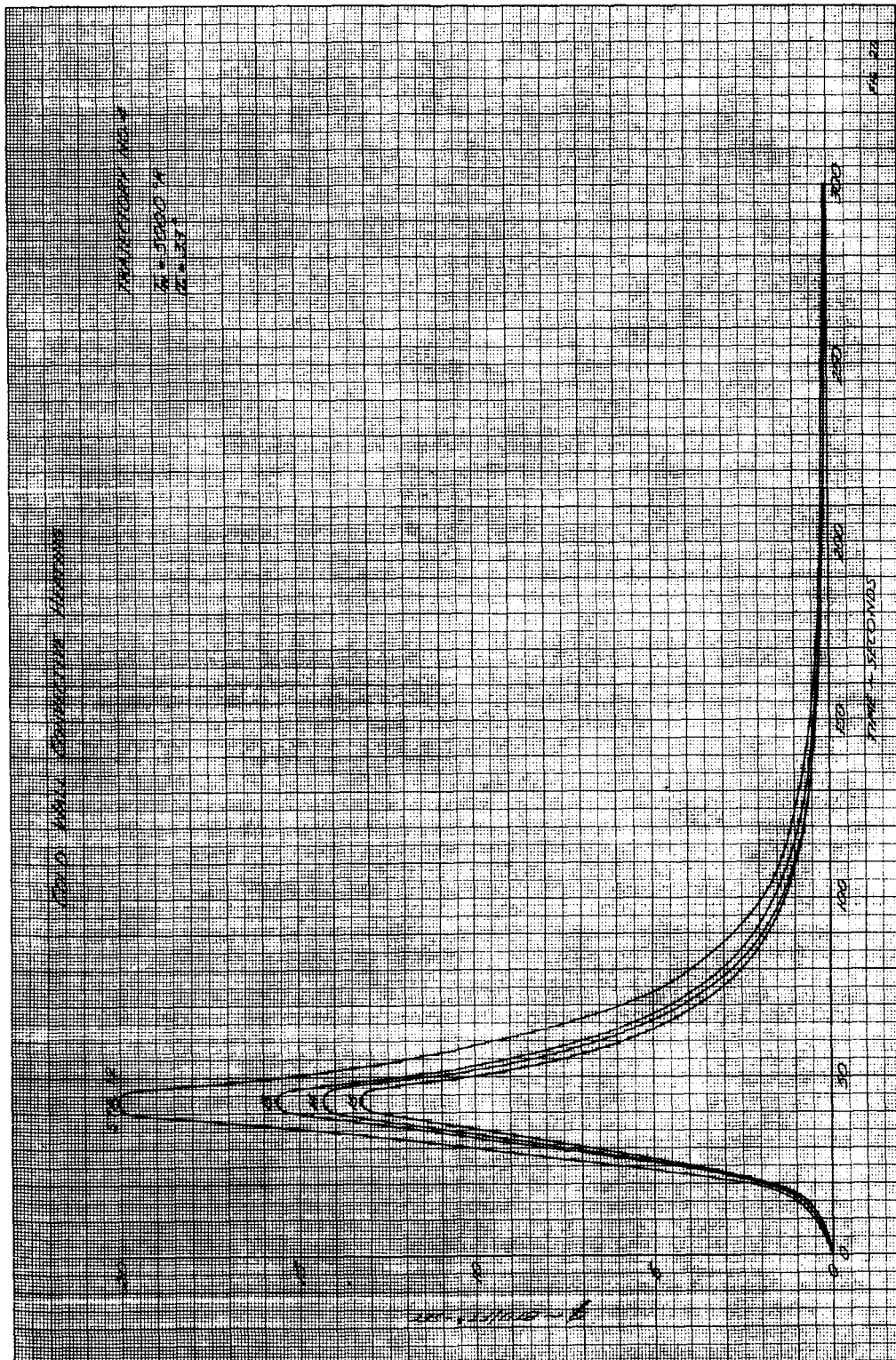Figure 20 COLD-WALL CONVECTIVE HEATING (PTS. 12-15, $a = 33^{\circ}$, TRAJ. 4)

-28-

AVCO
Research & Advanced Development
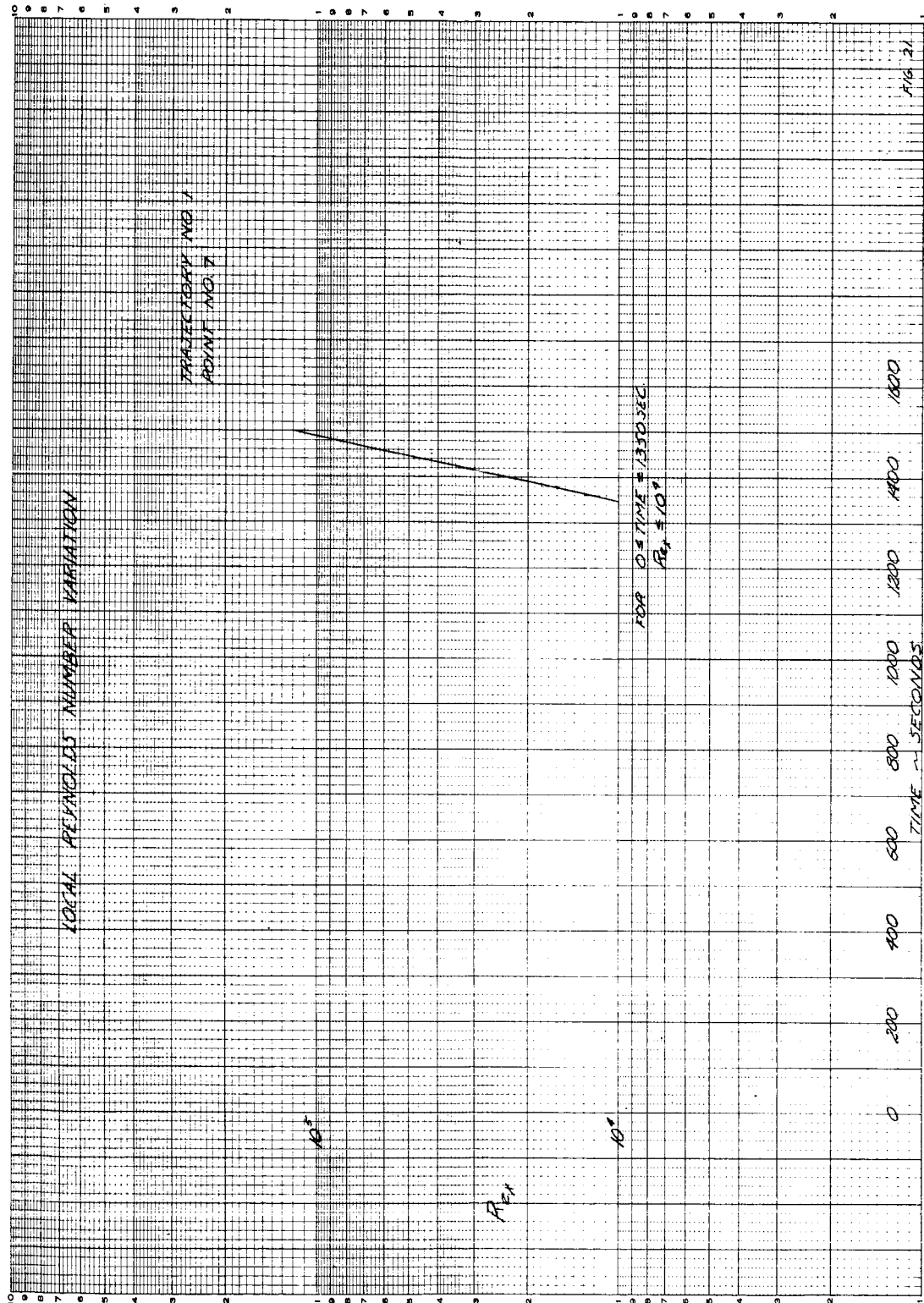
Figure 21 LOCAL REYNOLDS NUMBER VARIATION (TRAJ. NO. 1)
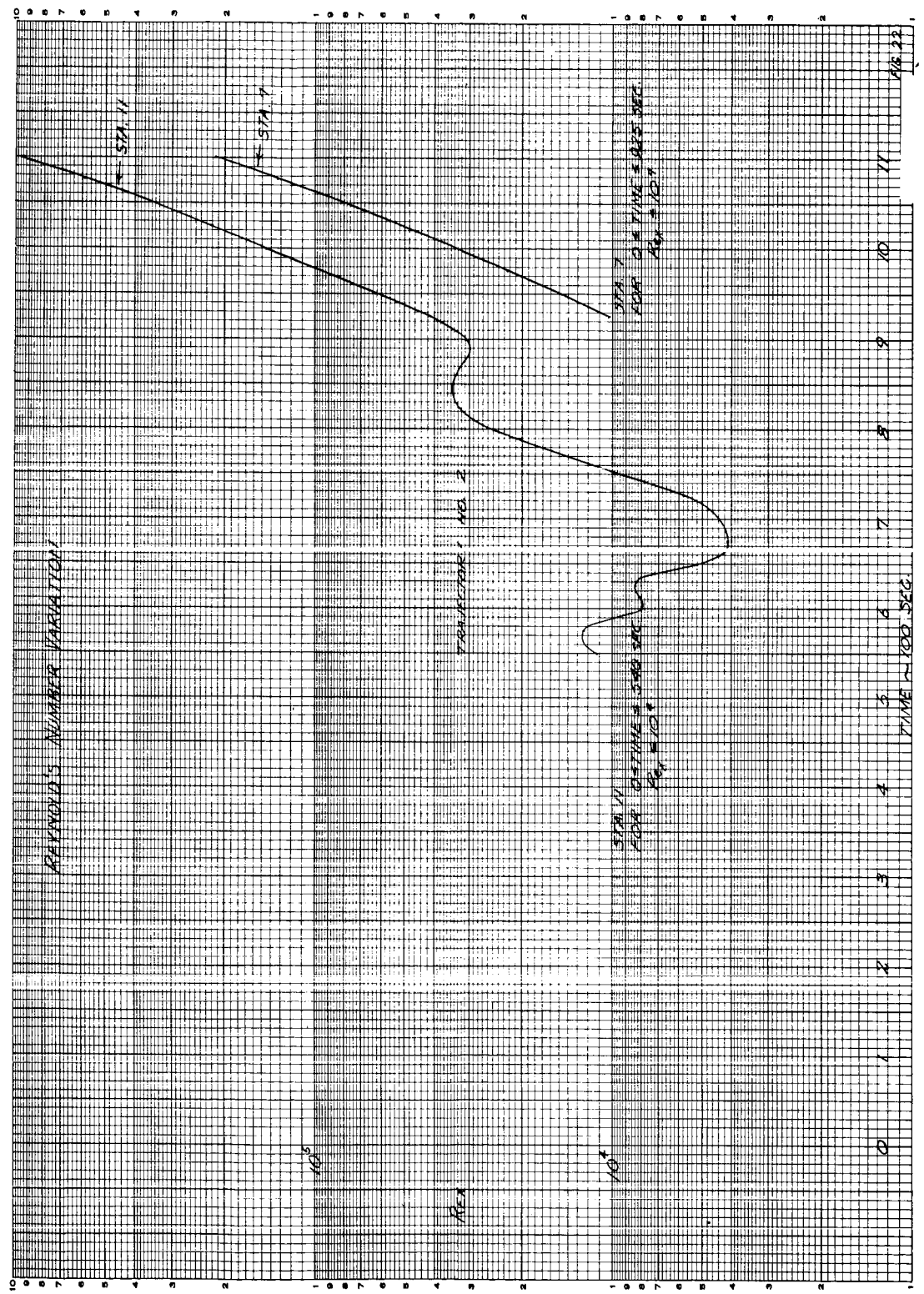
Figure 22 LOCAL REYNOLDS NUMBER VARIATION (TRAJ. NO. 2)

-30-

AVCO
Research & Advanced Development
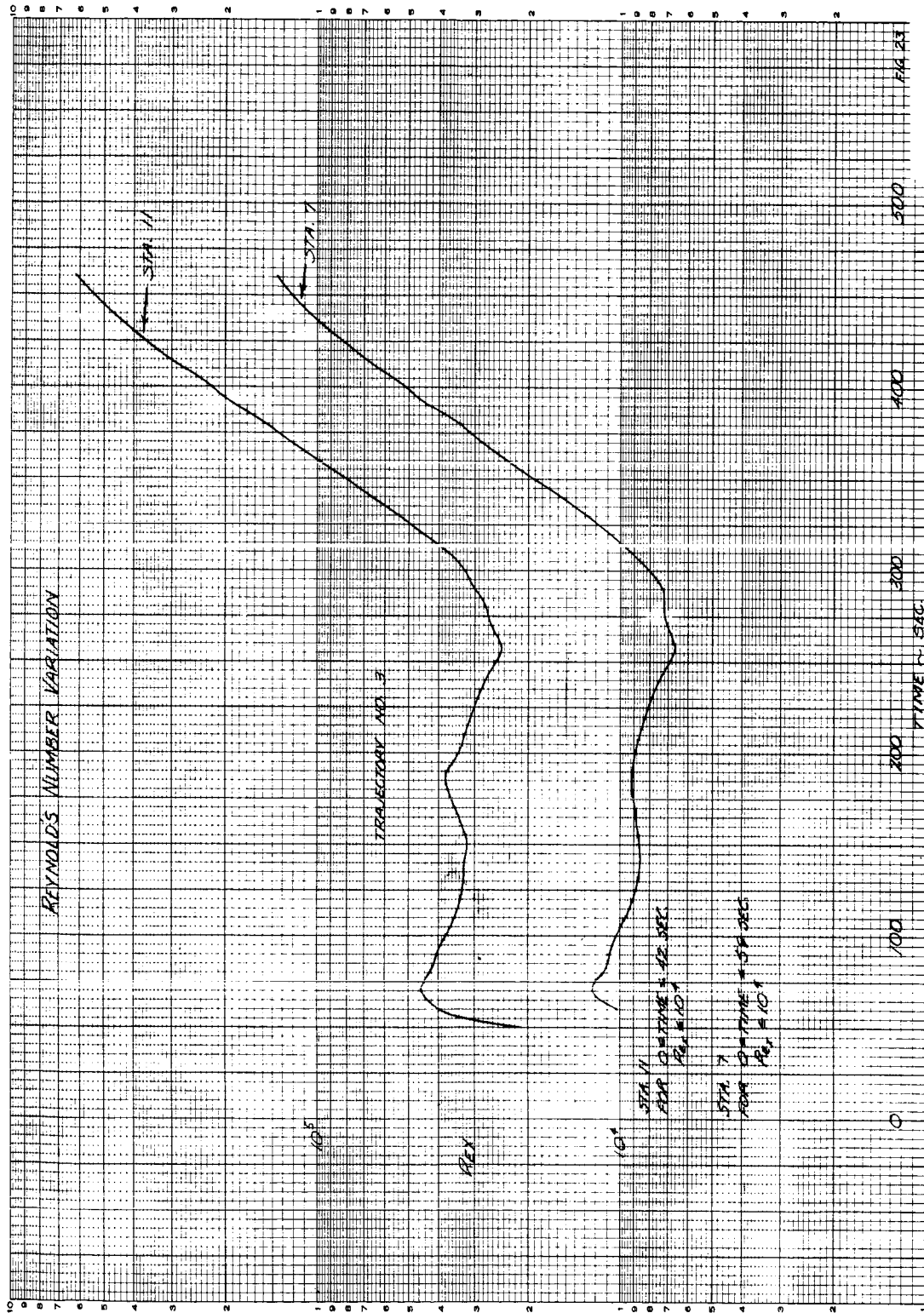
Figure 23 LOCAL REYNOLDS NUMBER VARIATION (TRAJ. NO. 3)

-31-
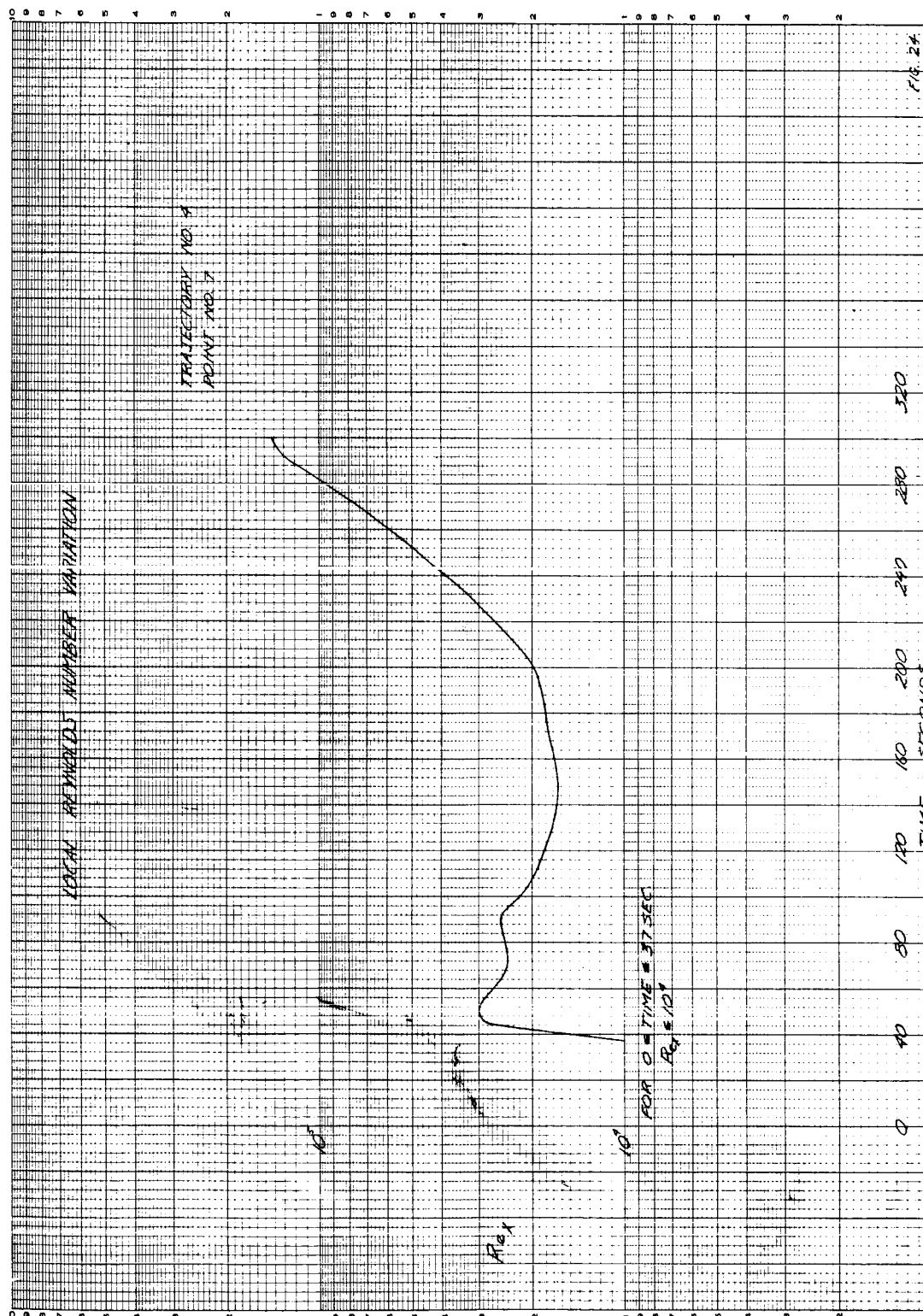
Figure 24 LOCAL REYNOLDS NUMBER VARIATION (TRAJ. NO. 4)

-32-

Figure 25 LOCAL REYNOLDS NUMBER VARIATION (TRAJ. NO. 5)

AVCO
Research & Advanced Development
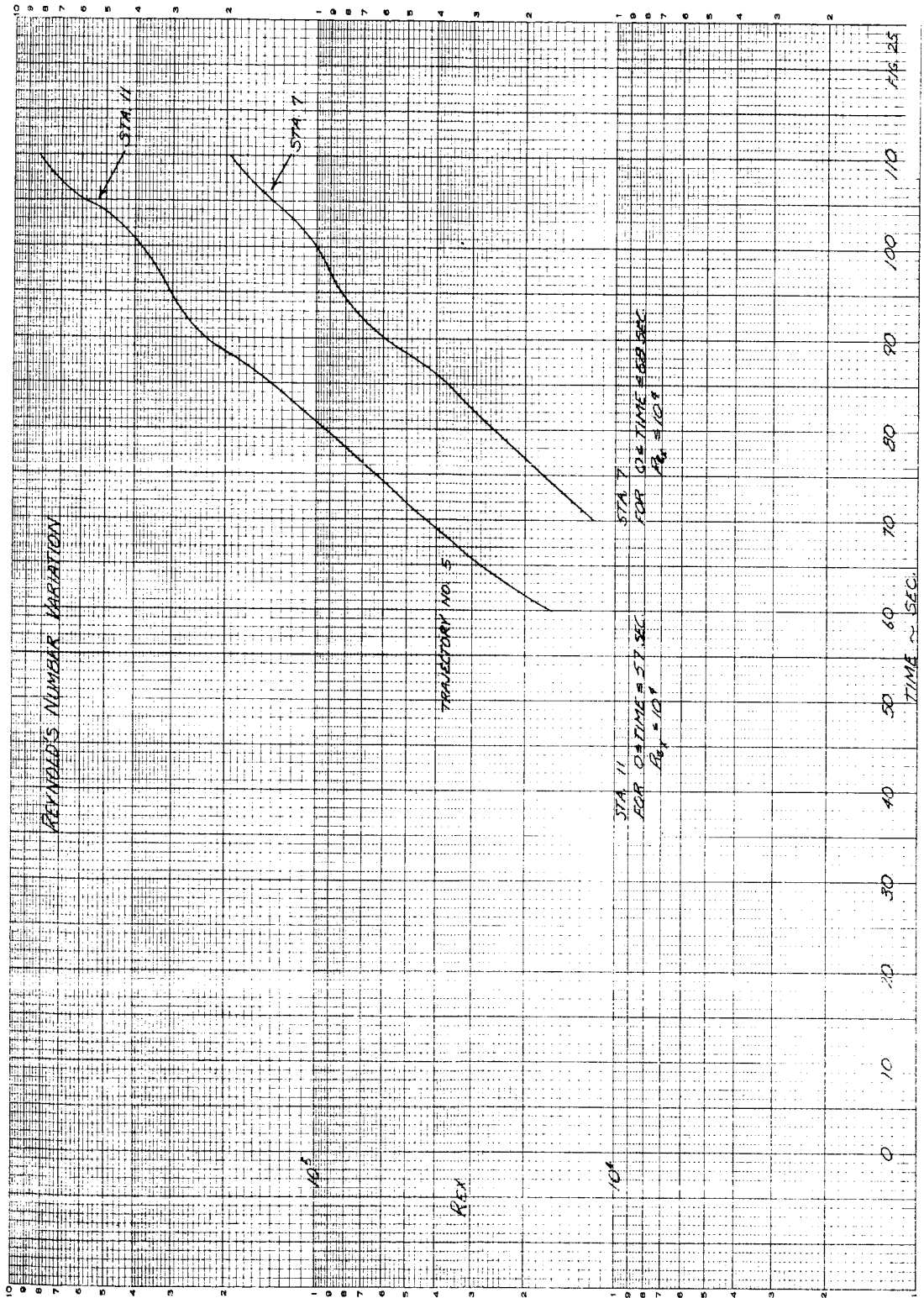
Figure 26 LOCAL REYNOLDS NUMBER VARIATION (TRAJ. NO. 6)

-34-

IV. RADIATIVE HEATING

Convective heat transfer is partially blocked by the ablation material entering the boundary layer. However the mass transfer will not block the radiant heating. Since mass transfer is dependent upon the total heat input to the body, a combined analysis coupling the radiative and convective heating is required. Actually the reaction of the material to radiative heating is a function of the spectral distribution of the radiant heat transfer. In this analysis the integrated value ove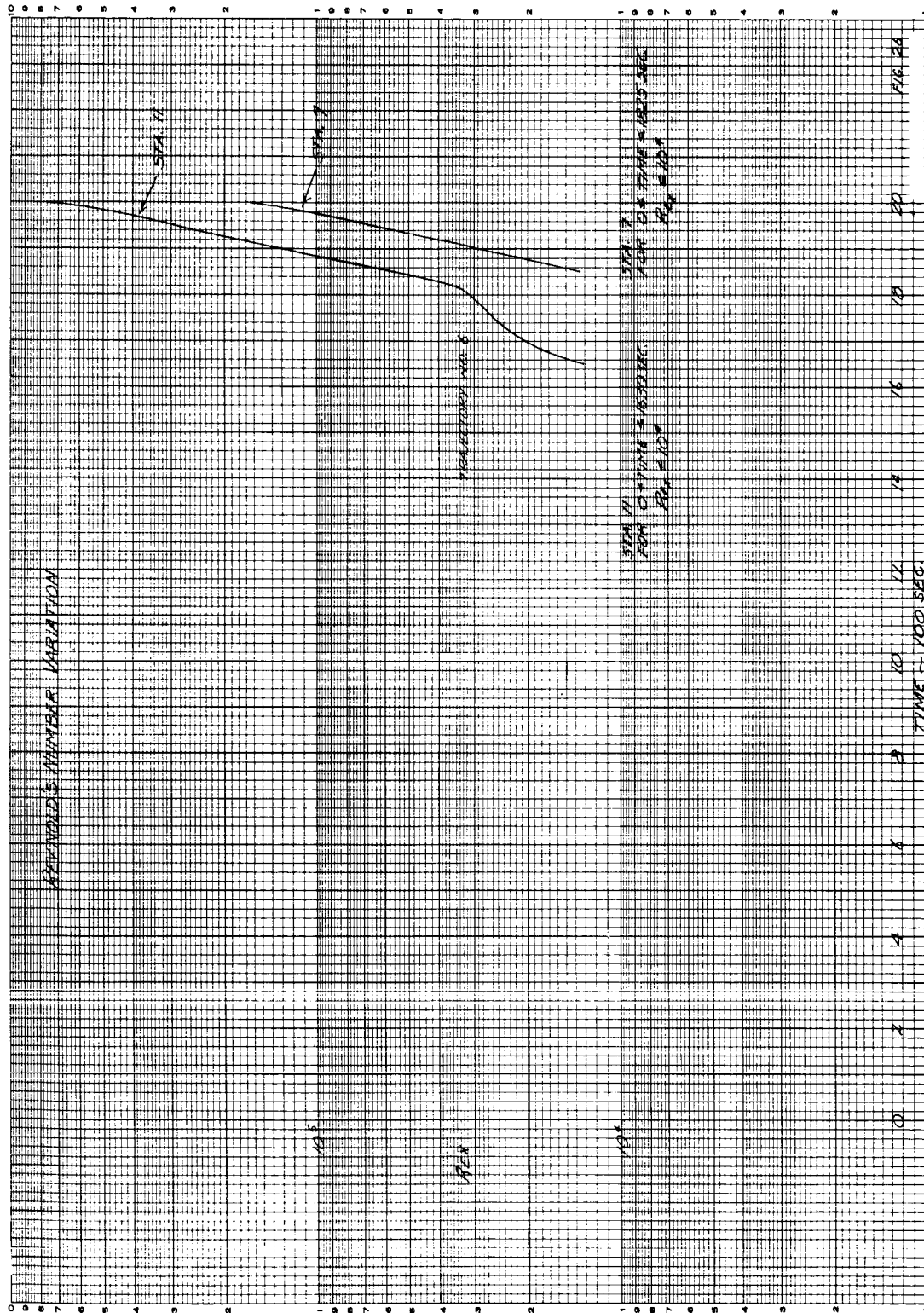r all frequencies is used 1) to determine the time interval in the trajectory during which radiation heating is important, and 2) to determine the shape of the radiant heat pulse.

The radiative heating is a direct function of the shock stand-off distance and shock shape. The semi-infinite slab assumption is utilized over the entire spherical face with the shock detachment distance measured normal to the body. The radiative heat transfer rate is therefore the product

$$\dot{q}_r = \epsilon_{eff} \, \sigma \, T^4 \, \Delta$$

The integrated values of the effective radiative emissivity are based on the works of Kivel and Bailey (reference 2). Shock detachment distance at the stagnation point is determined by correlating JPL schlieren test data (figures 27 and 28) with the theoretical calculations of Kaattari (reference 3). The shock stand-off distance to local body points away from the stagnation point is assumed to be linear with the normal shock-density ratio. The correlation between test and theory for shock shape is presented in figures 29 and 30. The shock shape for the present analysis is assumed to be independent of density ratio, and the test data shock shape is used in this analysis.

Working charts are available for estimating the emissivity of the air. However, these charts are time-consuming and cumbersome to use. To facilitate the calculations, an empirical equation has been fit to the Kivel and Bailey tables of radiative emissivity of air (reference 2):

$$\epsilon/cm \approx 5.85 \times 10^{-5} \, (\rho/\rho_0)^{1.15} \, e^{4.35(T/10^4)}$$

The fit is good to approximately 25 percent over the range of density ratios (ρ/ρ_0) of 10^{-4} to 10^{-1} and temperatures of $5,000°$ to $12,000°K$. The empirical curve fit to the Kivel and Bailey tables has been combined with linearized results of the shock detachment distance as a function of stagnation-density ratio resulting in the following approximation

AVCO
Research & Advanced Development
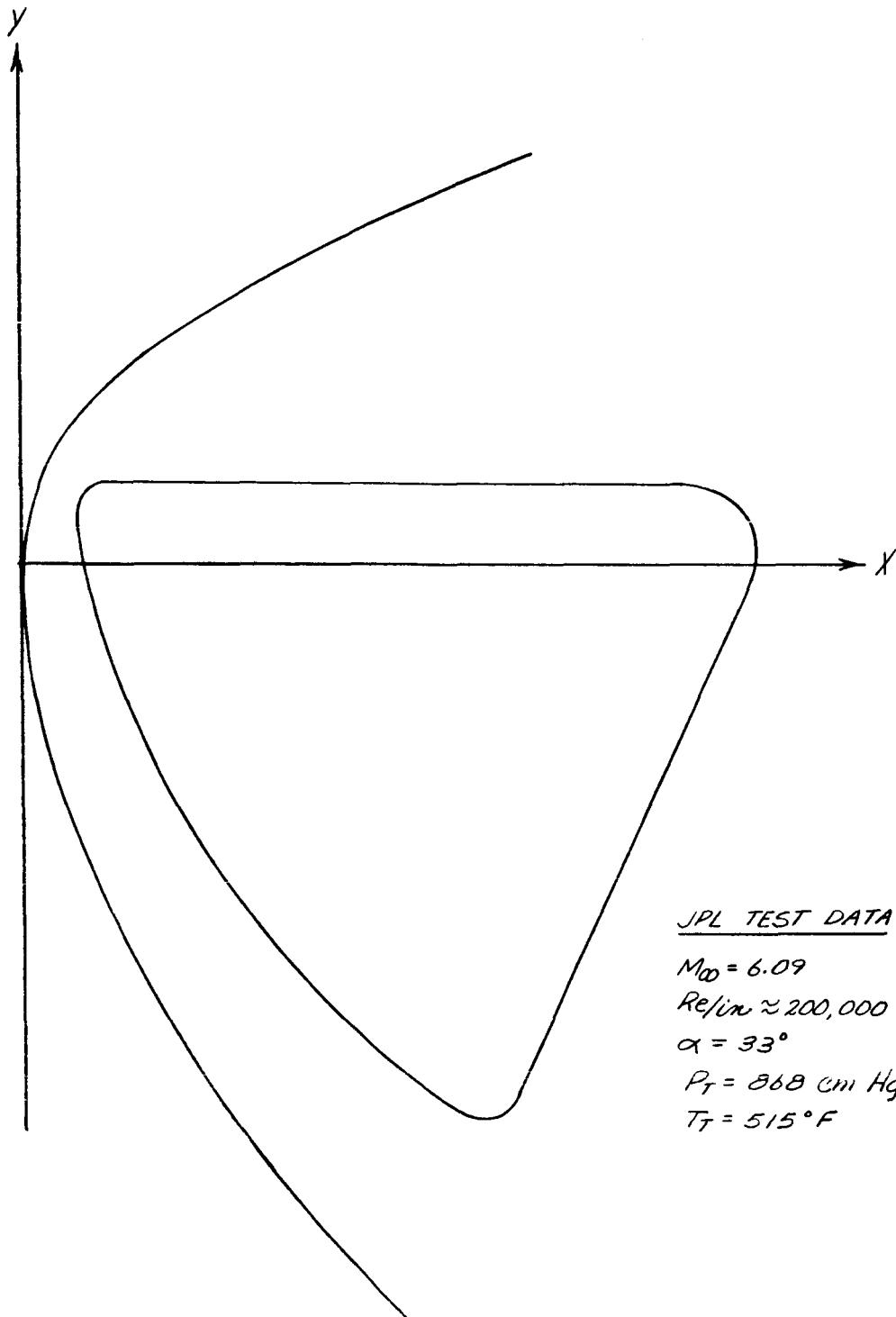
JPL TEST DATA

$M_\infty = 6.09$

$Re/in. \approx 200,000$

$\alpha = 33°$

$P_T = 868$ cm Hg

$T_T = 515°F$

Figure 27 SCHLIEREN PHOTOGRAPH TRACE NO. 1

AVCO
Research & Advanced Development

JPL TEST DATA

$M_{\infty} = 7.41$

$Re/_{in} = 93,128$

$\alpha = 33°$

$P_T = 1373$ cm Hg

$T_T = 1107$ °F
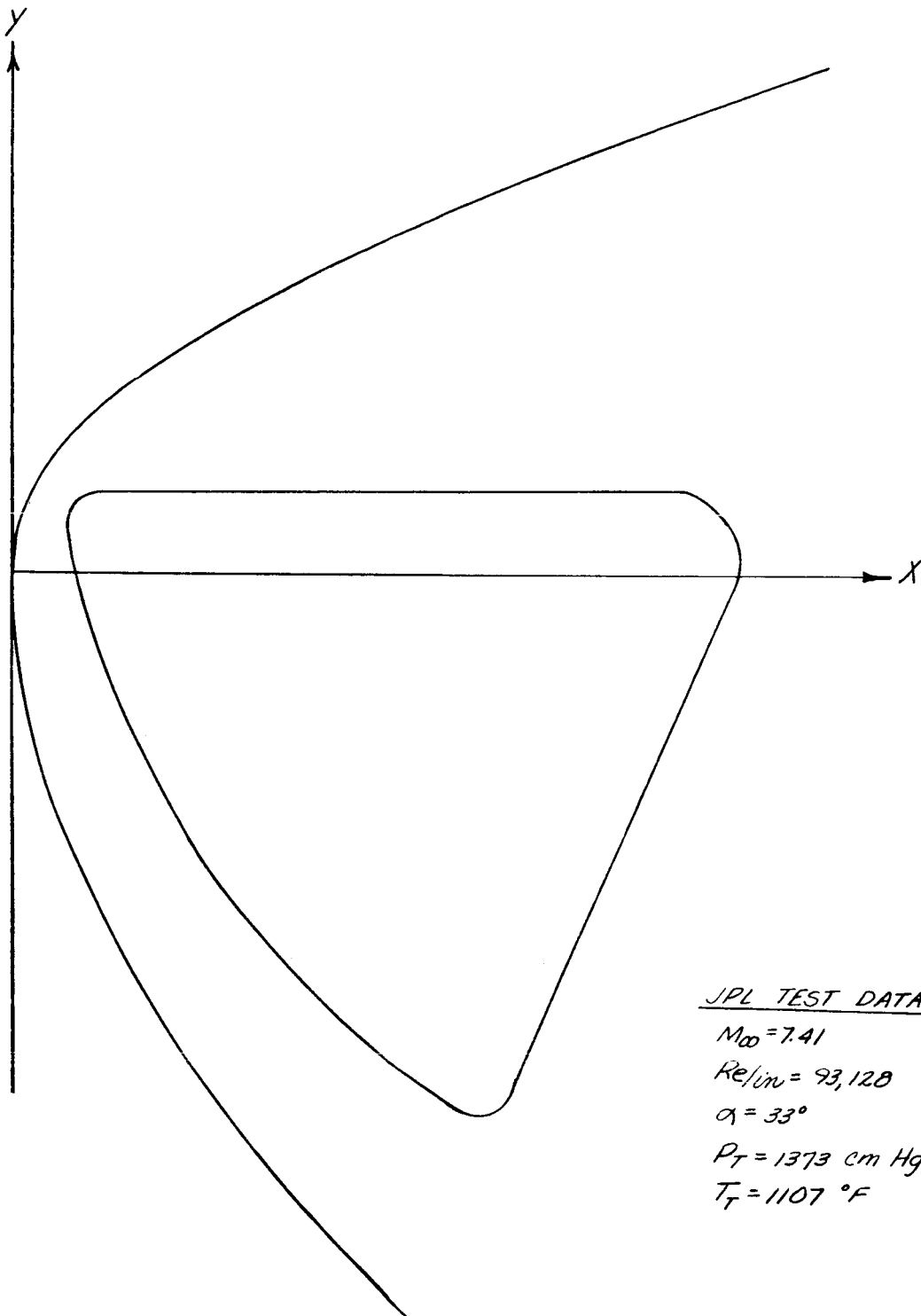
Figure 28 SCHLIEREN PHOTOGRAPH TRACE NO. 2

-37-

AVCO
Research & Advanced Development

Figure 29 SHOCK STAND-OFF DISTANCE

-38-

Figure 30 SHOCK SHAPE

-39-

$$\dot{q}_r \approx 131 \, K' \, \frac{\rho_\infty/\rho_0}{\rho_s/\rho_0} \left(\frac{\rho_{field}}{\rho_0} \right)^{1.15} \left(\frac{T_{field}}{10^4} \right)^4 e^{4.35 \, (T/10^4)}$$
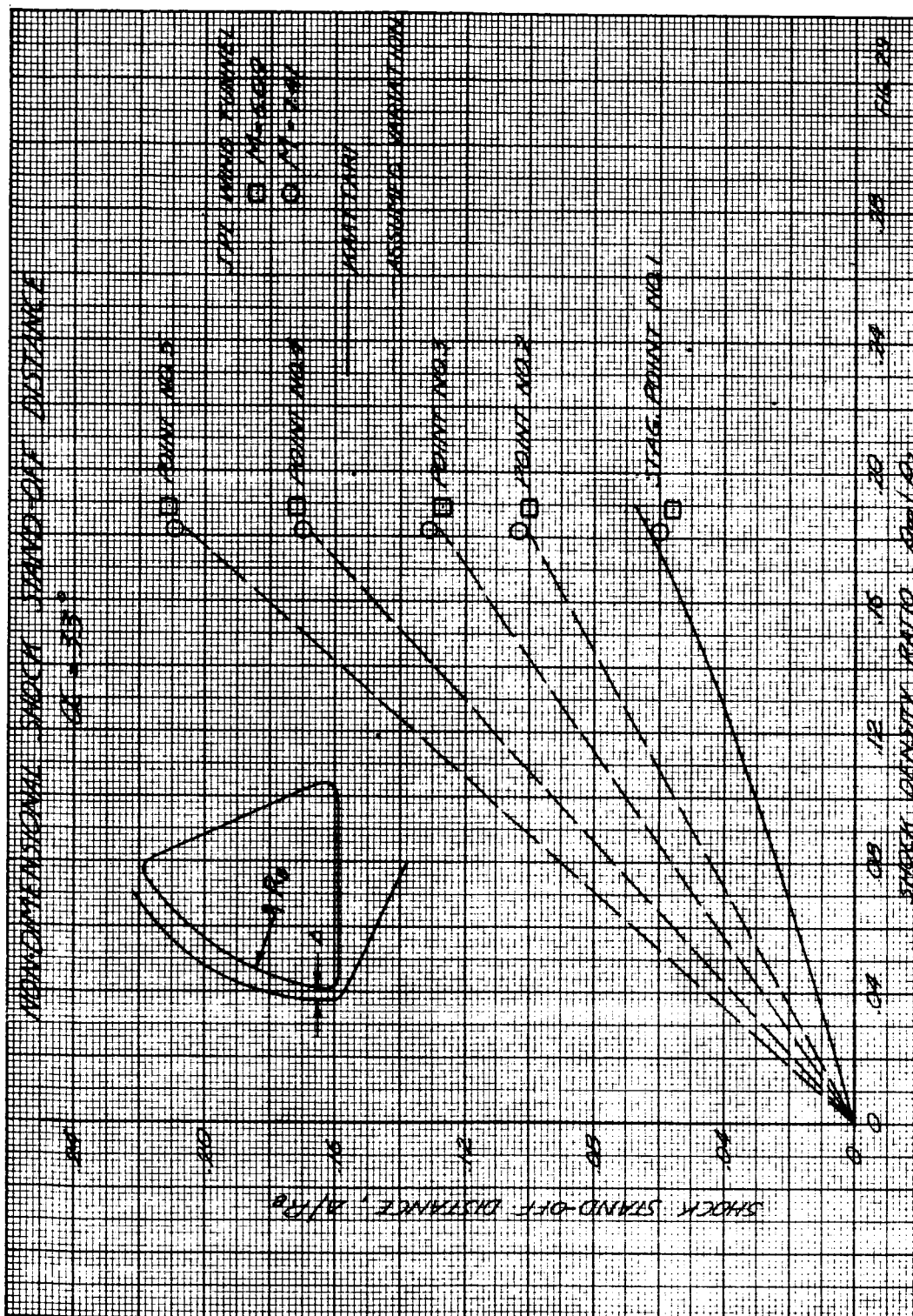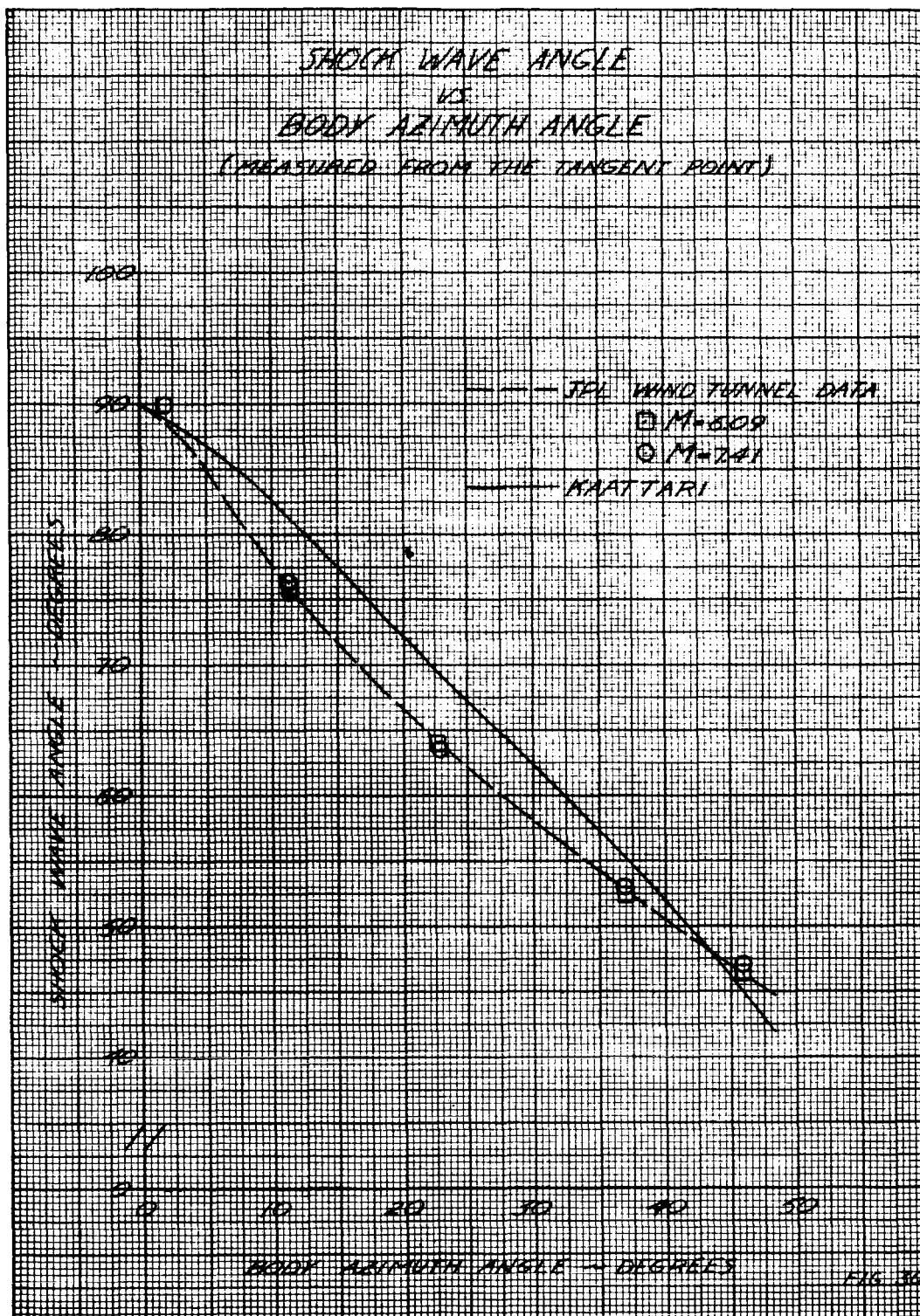
where $K' = d\left(\frac{\Lambda}{R_B}\right) \Big/ d\left(\frac{\rho_\infty}{\rho_s}\right)$ as determined from figure 29. The terms ρ_{field} and T_{field} refer to the temperature and density at any point in the field (constant in a given slab).

The radiative heat flux is presented in figures 31 and 32 at the stagnation point for trajectories 1 and 4 respectively. The accuracy of the empirical fit for the range of densities and temperatures associated with these trajectories is approximately ± 10 percent. Presently under analysis are the works of Thomas (reference 8) who has recomputed the emissivities of air based on the absorption coefficients of Meyerott (reference 9) (See figures 31 and 32). These results differ from Kivel and Bailey's by a factor of 2. Until test data on radiative heating become available, we will continue to use Kivel and Bailey since their results are conservative.

The radiative heating-time histories for Points 1, 2, 3, 4, and 5 on the spherical face are presented in figures 33 and 34. The slab has been assumed to be tangent to the body point in question. Since the properties vary normal to the body, the arithmetic mean radiation between the body surface and shock wave has been assumed. In essence the field has been divided into two slabs with slab 1 possessing the properties behind the shock wave and slab 2 possessing the properties of the body surface.

The radiative heating distribution in nondimensional form along the zero meridian on the spherical face is presented in figure 35. Contrary to thought, the radiative heating increases on the leeward side of the stagnation point. This initial increase is caused by the combined effect of the small decreases in local flow-field properties and a large increase in shock-detachment distance.

All other specified points (figure 1) receive negligible radiation because of the relatively low densities and temperatures and are not analyzed.
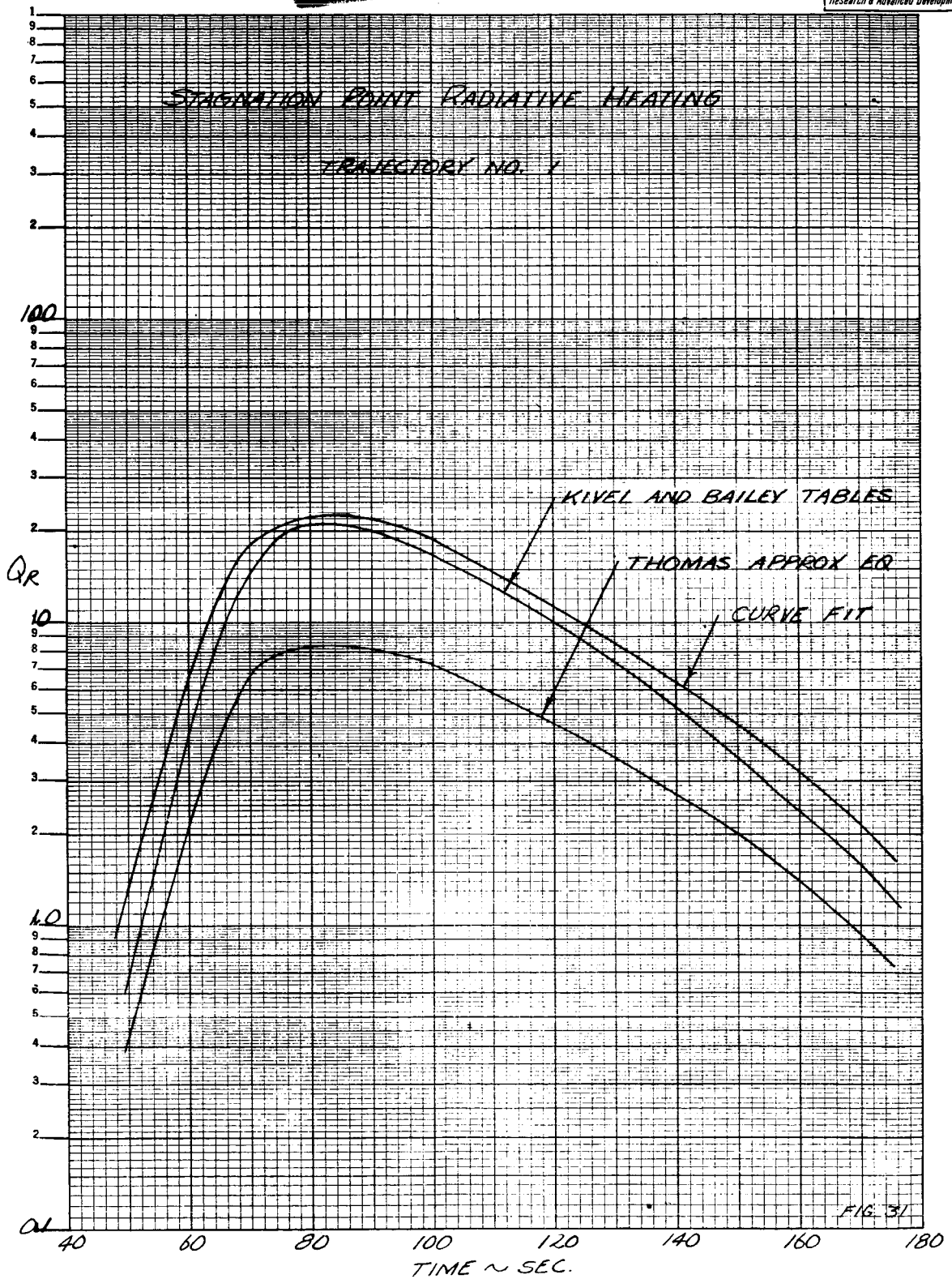
Figure 31 STAGNATION-POINT RADIATIVE HEATING (TRAJ. 1)

-41-
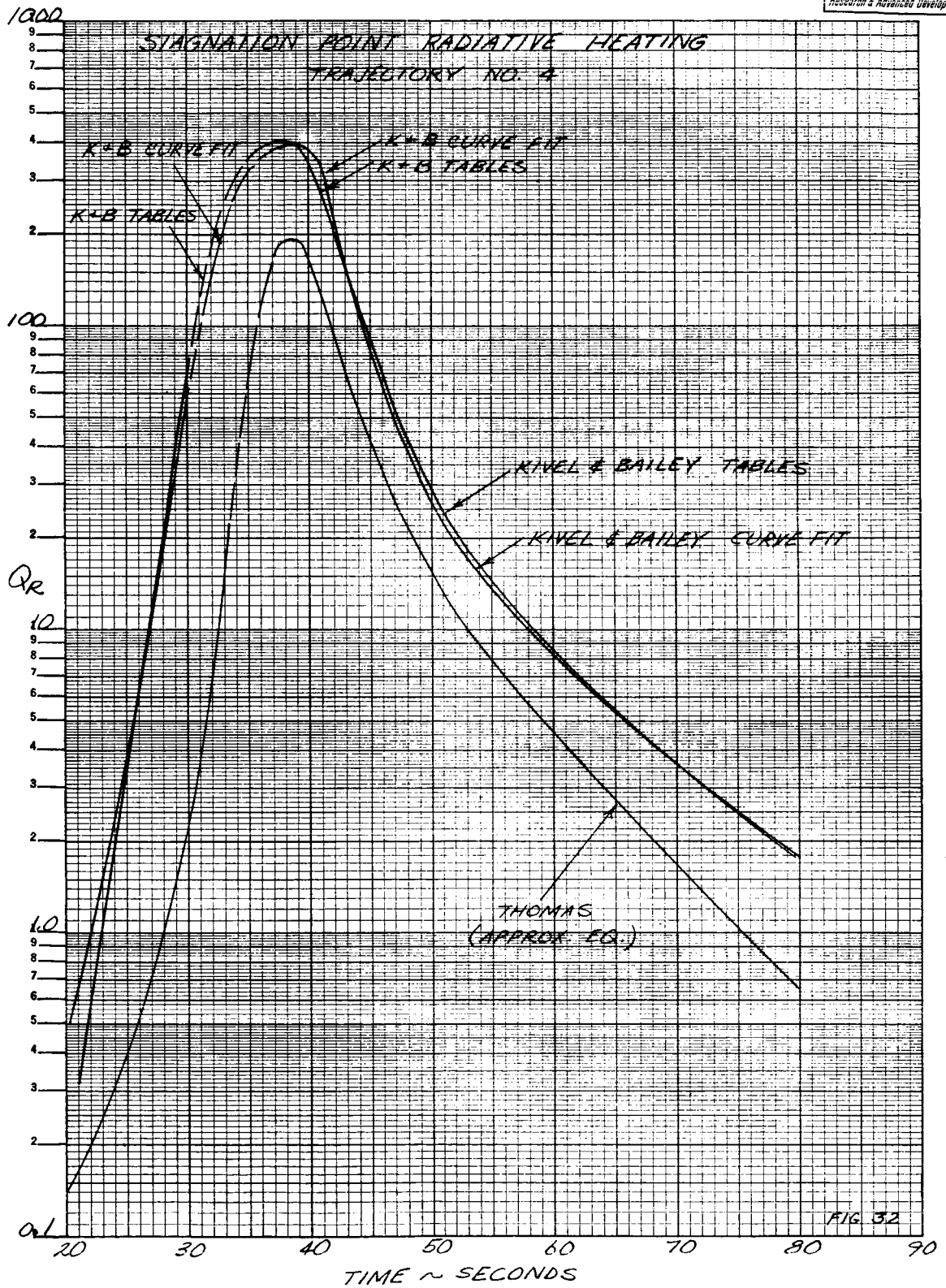
Figure 32 STAGNATION-POINT RADIATIVE HEATING (TRAJ, 4)

-42-

AVCO
Research & Advanced Development
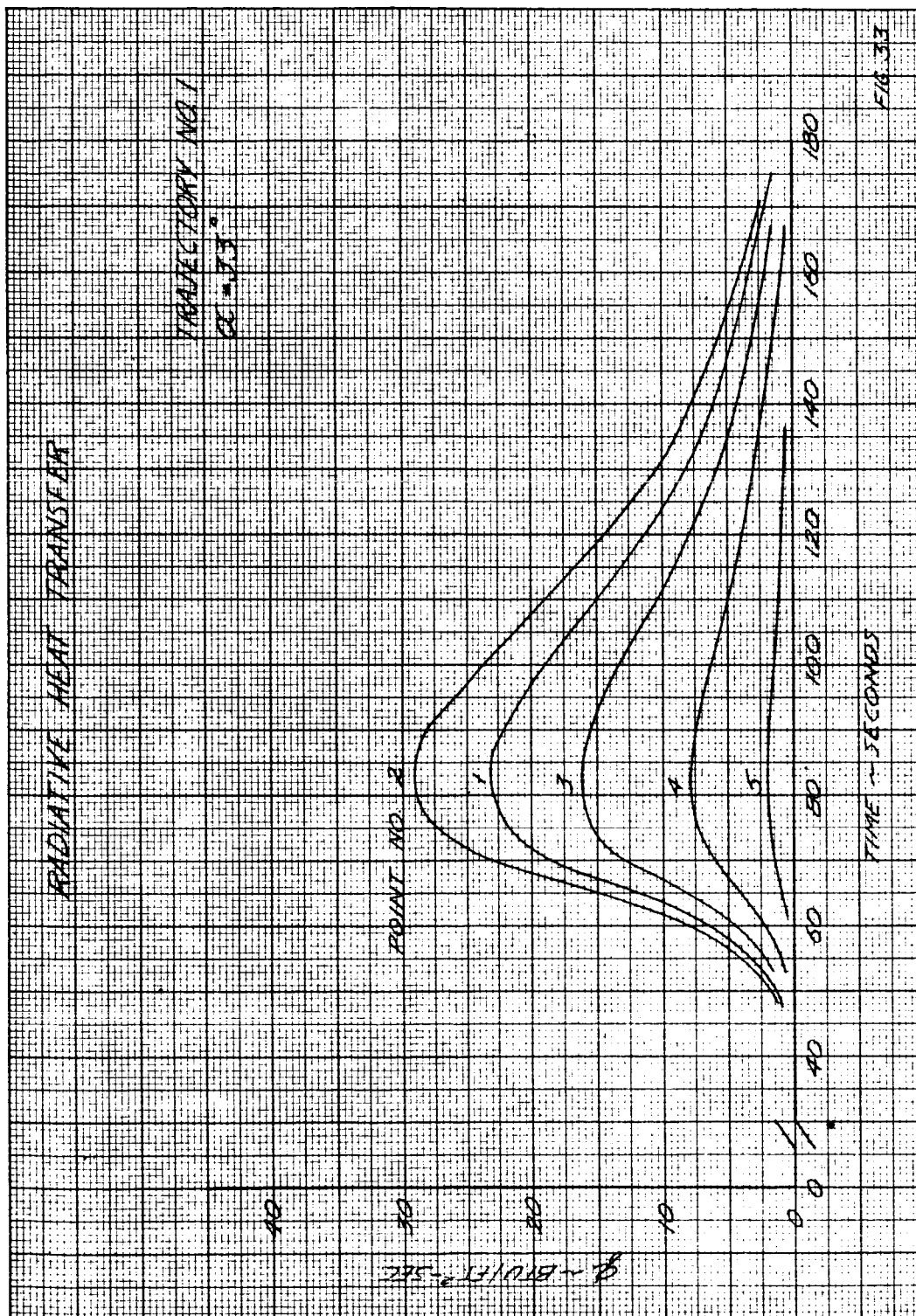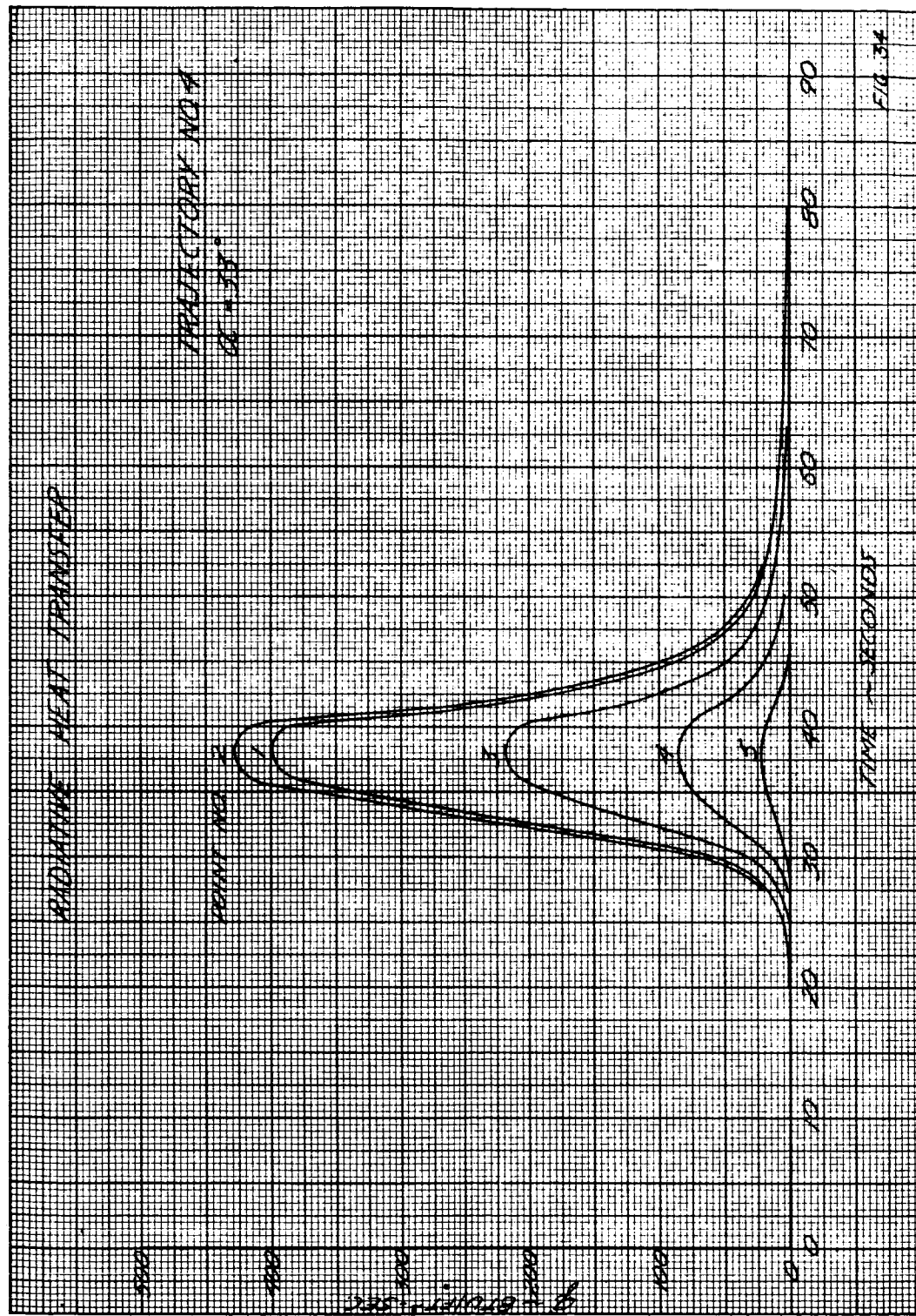

Figure 33   RADIATIVE HEATING (PTS. 1-5, TRAJ. 1)

Figure 34 RADIATIVE HEATING (PTS. 1-5, TRAJ. 4)

Figure 35 LONGITUDINAL RADIATIVE HEAT-TRANSFER DISTRIBUTION
($a = 33°$, $\phi = 0°$)

-45-

V. COMPARISON OF THEORY AND TEST

Experimental heating distributions around the Apollo command module have been obtained in the Avco 1.5-inch shock tube. The shock tube consists of a 1.5-inch diameter, 3-foot length, high-pressure driver connected to a 1.5-inch diameter, 16-foot length driven section. The high-pressure driver uses a combustion mixture of oxygen, hydrogen and helium to create strong shock waves. The stagnation reservoir condition range is 30 to 300 atmospheres of pressure and enthalpies (H/RT_0) of 50 to 900.

The present shock-tube tests are designed for laminar convective heating. Radiative heating does not exist because of the relatively low temperature associated with the nominal reservoir conditions.

The nominal test conditions are:

M_{shock} = 7.7 H_t/RT_o = 92

P_1 = 5 cm Hg T_t = 4150°K

T_1 = 300°K P_t = 2400 cm Hg - 30.3 atm.

$R_{e\infty}$ = 1.6 x 10⁵/cm

The simulated flight conditions are approximately:

Alt = 55,000 ft

Vel = 12,000 ft/sec

The instrumentation used exclusively is the thin-film resistance thermometer gage with resulting data accuracy of $\pm$ 15 percent. Both the standard (0.40-inch wide) and new (0.005-inch wide) gages were employed in the tests. The small gages permitted extensive surveys around the transition shoulder and in the vicinity of the stagnation point.

The "raw" test data was corrected to cold-wall conditions to permit proper correlation with the cold-wall theoretical results. The resulting data correction when presenting the cold wall convective heating ratio of the cold wall heating to the cold wall stagnation point heating at an angle of attack of zero degrees is

$$\left(\frac{\dot{q}}{\dot{q}_s}\bigg|_{\alpha=0}\right)_{cw} = \left(\frac{\dot{q}}{\dot{q}_s}\bigg|_{\alpha=0}\right)_{test} \left(\frac{1 - H_w/H_s}{\dfrac{H_r}{H_s} - \dfrac{H_w}{H_s}}\right)$$

-46-

The H_t/H_s ratio was determined with the use of perfect gas relationships. For the nominal test conditions this ratio is 0.054.

The experimental and theoretical results are compared in this nondimensional form. The zero-degree stagnation-point heating rate associated with the test data is experimentally determined, and the value associated with the theoretical results is predicted by Fay and Riddell (reference 4) with the experimentally determined correction of Boison (reference 10) applied to the spherical radius. The effective radius for the spherical segment is 134 inches.

Comparisons between the experimental and theoretical heating distributions are presented in figures 36 to 39. The longitudinal heat-transfer distribution for the zero meridian is presented in figure 36 for two Mach numbers 31 and 2.09.

The longitudinal heat transfer distribution for the transition shoulder is presented in more detail in figure 37.

Circumferential heat-transfer distributions on the conical afterbody are presented (figures 38 and 39) for two axial locations (S/R = 1.4 and 2.0).

Heat transfer rates presented in nondimensional form are essentially independent of Mach number and gas composition, similar to the nondimensional pressure distribution.

In general comparisons between theory and test are in excellent agreement (± 10 percent). A discrepancy does exist between the theoretical and experimental stagnation-point heating rates. The reason for this discrepancy is that the assumed location of the theoretical stagnation point and experimental value do not coincide. The stagnation point has been determined experimentally at low Mach number only. A theoretical prediction of the stagnation point location for various Mach numbers is not available at this time.

Recent JPL pressure data (figure 4) for the Mach number range of 6 to 9 shows that the stagnation point is not located at the forward tangent point (body point 1), but that it is located on the spherical face. Avco shock-tube heating data (figure 36) for a relatively low Mach number ($M_\infty = 2.0$) also show the stagnation point location to be on the spherical face.

The present theoretical method of predicting the stagnation heating is a function of the stagnation point location. Therefore, the location of the stagnation point on the spherical face would result in a lower heating rate as shown by the experimental data (figure 36). Since the effect of Mach number is unknown at this time, the theoretical heating rates shown in figures 2 and 3 should be used in preliminary design, although they appear to be conservative.

Figure 36 COMPARISON OF LONGITUDINAL CONVECTIVE HEAT-TRANSFER DISTRIBUTIONS ($\alpha = 33^\circ$, $\phi = 0^\circ$)
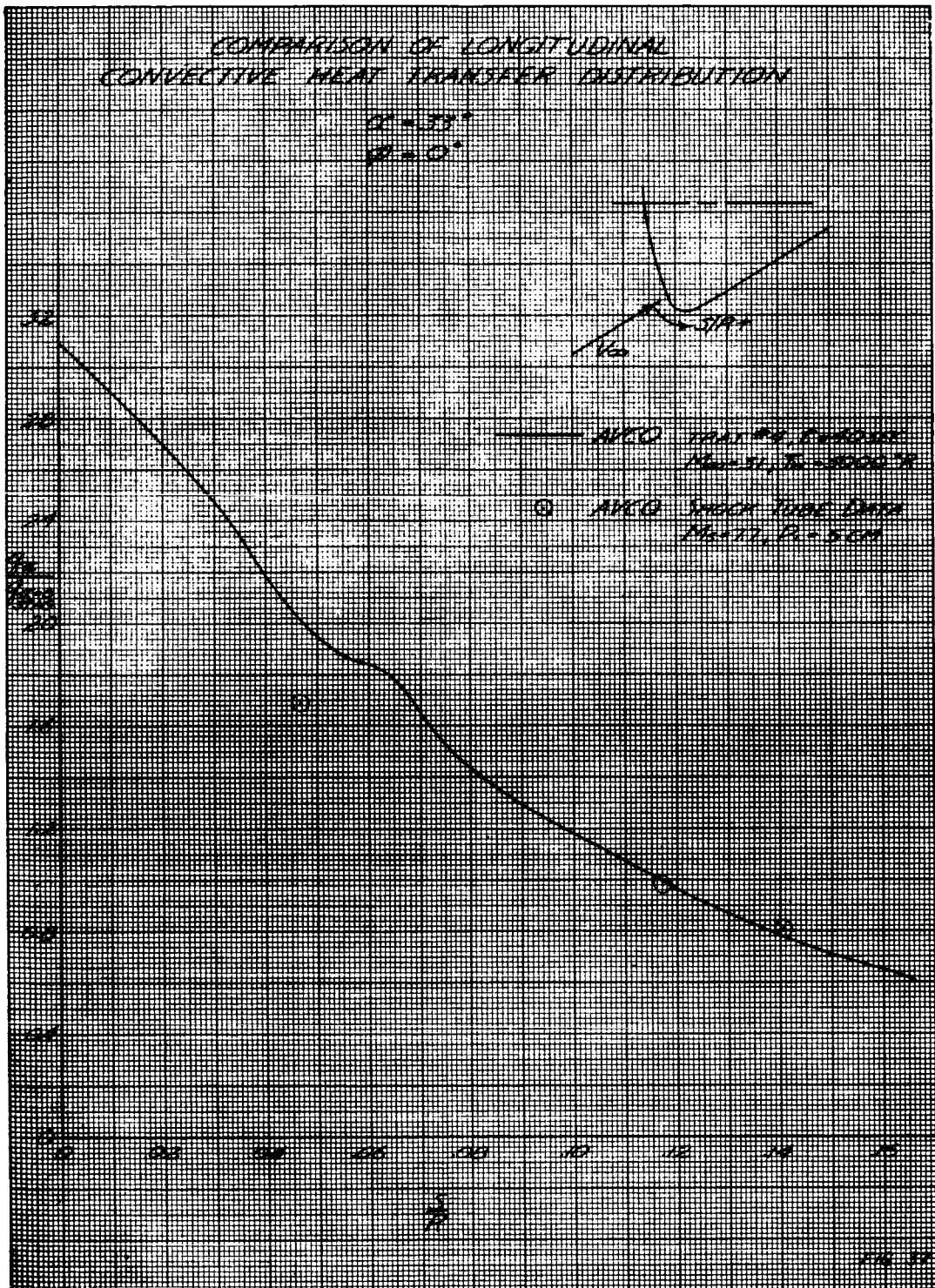
Figure 37 COMPARISON OF LONGITUDINAL CONVECTIVE HEAT-TRANSFER
DISTRIBUTIONS (TRANSITION SHOULDER)

-49-

Figure 38 COMPARISON OF CIRCUMFERENTIAL CONVECTIVE HEAT-TRANSFER
DISTRIBUTIONS (S/R = 1.4, α = 33°)
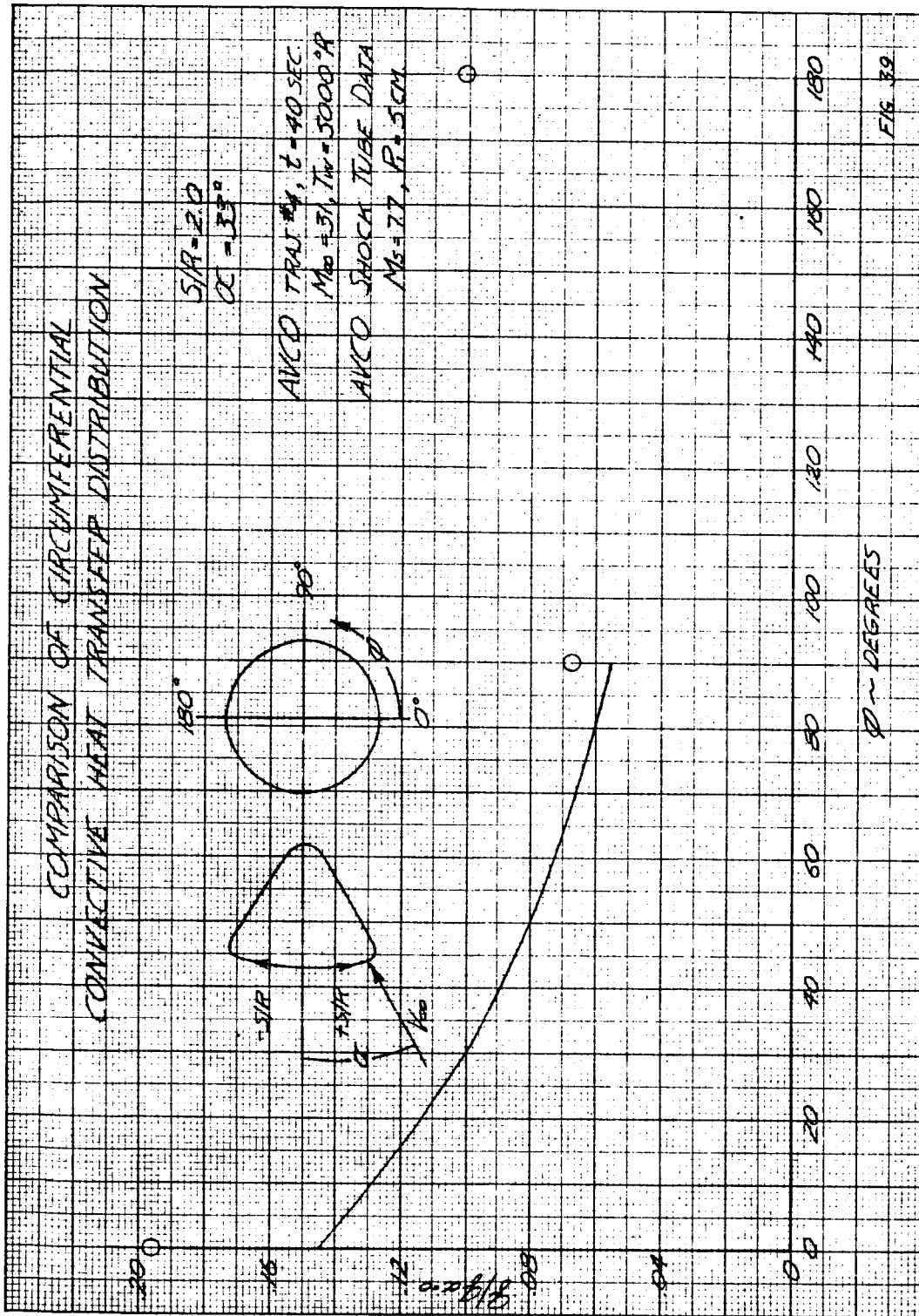
Figure 39 COMPARISON OF CIRCUMFERENTIAL CONVECTIVE HEAT-TRANSFER
DISTRIBUTIONS (S/R = 2, α = 33°)

Studies are being conducted to develop a new approach for the convective heating of three-dimensional, nonaxisymmetric stagnation points. It is to be noted that the change in stagnation point heating should not affect any of the other theoretical heating distributions.

VI. CONCLUSIONS

Comparisons made to date between theory and test indicate that the present theoretical methods are a valid approach for preliminary vehicle-design analysis. Other areas of future work will include studies of the convective heating on the leeward meridian, and the nonequilibrium effects on convective and radiation heating.

REFERENCES

1. NAA Procurement Specification, MC 364-0001, Apollo Command Module Heat-Shield Ablative Panels (21 March 1962).

2. Kivel, B., and K. Bailey, Tables of Radiation from High Temperature Air, Avco Everett Research Laboratory, Research Report 21 (December 1957).

3. Kaattari, G., Predicted Shock Envelopes About Two Types of Vehicles at Large Angles of Attack, NASA TN-D 860 (April 1961).

4. Fay, J. A., and F. R. Riddell, Theory of Stagnation Point Heat Transfer in Dissociated Air, Avco Everett Research Laboratory, Research Report 1 (April 1957).

5. Reshotko, E., Heat Transfer to a General Three-Dimensional Stagnation Point, Jet Propulsion, pp. 58-60 (January 1958).

6. Kemp, N., P. Rose, and R. Detra, Laminar heat transfer around blunt bodies in dissociated air, J. Aerospace Sci. 26 pp, 421-430 (1959).

7. Eckert, E., Engineering relations for heat transfer and friction in high velocity laminar and turbulent boundary layer flow over surfaces with constant pressure and temperature, ASME Paper No. 55-A-36.

8. Thomas, P., Air emissivity and shock layer radiation, J. Aerospace Sci. 29 pp. 477-478 (1962).

9. Meyerott, R. E., J. Sokoloff, and R. A. Nicholls, Absorption Coefficients of Air, Geophysics Research Paper 68, AFCRC, Bedford, Mass. (1960).

10. Boison, J., and H. Curtiss, An experimental investigation of blunt body stagnation point velocity gradient, ARS J. 26 pp, 130-135 (1959).

DISTRIBUTION

Addressee	No. of Copies
NAA/S&ID, Attn: J. M. Kerr (+ 1 reproducible)	25
Central Files	1
Document Control	5
Research Library	2
Apollo Central File (+ 1 reproducible)	10
I. Sacks	1
E. E. H. Schurmann	1
H. Weisblatt	1
B. Henshall	1
A. Pallone	1
A. Hanawalt	1
J. Boehringer	1
J. Graham	1
J. Stevens	1
H. Hurwicz	1
H. Tereshkow	1
F. Diederich	1
M. C. Adams	1
C. Berninger	1
E. Offenhartz	1
P. Andrews	1
M. Kaplan	1
E. G. Lowery, NAA Resident Representative	1
J. Collins	1
R. X. Hugghin	1
T. Sellers	1
D. Liu	1
R. Gustafson	1
N. Thyson	1
W. Zeh	1